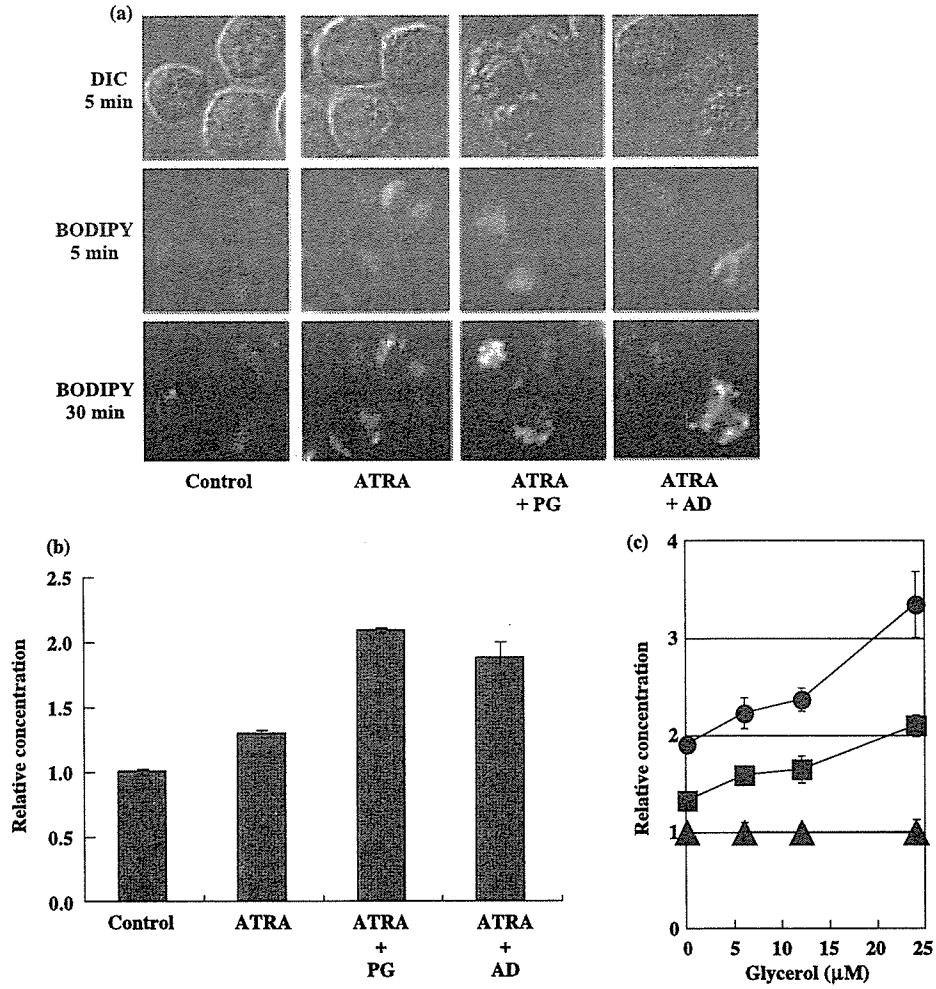

Fig. 7. (a) Intracellular distribution of BODIPY-FL-C12 fluorescence in differentiated and untreated NB4 cells. Cells were treated for 3 days with all-trans retinoic acid (ATRA; 1 μM), ATRA (1 μM) + 15-deoxy-Δ12,14-prostaglandin J2 (PG; 4 μM) or ATRA (1 μM) + AD (AD4833, 50 μM). Cells were incubated in medium containing BODIPY-FL-C12 for 2 min at room temperature and were subsequently chased and examined using a fluorescence microscope. Upper panels are difference interference contrast images. Middle and lower panels are the corresponding fluorescence microscopy images. BODIPY, BODIPY-FL-C12. Bar, 10 μm. (b) Relative concentration of triacylglycerol containing BODIPY-FL-C12 in NB4 cells. Cells were treated for 3 days with peroxisome proliferator-activated receptor γ (PPARγ) ligand (PGJ2 4 μM, AD4833 50 μM) and/or ATRA (1 μM). The assay methods are described in Materials and methods. Values represent mean ± SD. The relative concentrations of triacylglycerol containing BODIPY-FL-C12 in differentiated cells were calculated as fluorescence strength compared to that in untreated cells taken as 1.00. (c) Triacylglycerol synthesis activity in NB4 cells. Cells were treated for 3 days with PPARγ ligand (PGJ2 4 μM, AD4833 50 μM) and ATRA (1 μM). The method of the enzyme assay is described in Materials and methods. Values are mean ± SD. The relative concentrations of triacylglycerol containing BODIPY-FL-C12 in differentiated cells are plotted together with that of untreated cells taken as 1.00. (●), ATRA + PG; (■), ATRA + AD; (▲), control.

differentiation of normal and malignant myeloid cells (especially monocytic cells) and demonstrated that troglitazone combined with a retinoid was a moderately potent inhibitor of the clonogenic growth of acute myeloid leukemia cells, but not a potent inducer of differentiation of these leukemia cells (Asou *et al.* 1999). Our results clearly indicated that combined treatment with PPARγ ligand and ATRA induced differentiation of NB4 cells. This discrepancy between these findings may be related to the fact that in the study of Asou *et al.* (1999), NB4 cells were treated with troglitazone (10^{-5} M) as the PPARγ ligand, and the concentration of troglitazone was rather low compared to our conditions. We also examined the effects of PPARγ ligands and ATRA on HL-60 cells and observed synergistic effects of PPARγ ligands

on the induction of differentiation and lipogenesis, as in NB4 cells.

The basis for differentiation therapy of acute leukemia is the treatment of cells with several physiological agents at low concentration because high doses of single agents might provoke the side-effects of the agents and the resistance to the induction of differentiation. In this study, when PPARγ ligands were used alone, differentiation did not occur, but the combination of PPARγ ligand and ATRA synergistically promoted the differentiation of NB4 cells. The observed cooperativity between PPARγ ligands and ATRA has important implications for the use of combinations of these agents in differentiation therapy. PPARγ, like many members of the nuclear hormone receptor superfamily, functions as a heterodimer with the RXR. Recent studies have identified two types of RXR-dependent heterodimers: non-permissive and permissive (Schulman *et al.* 1998; Westin *et al.* 1998). In non-permissive heterodimers, such as those between RXR and RAR, the partner actively interferes with the ability of RXR-specific ligands. In contrast, permissive heterodimers, such as RXR-PPARγ, allow RXR signaling. In the current study, we demonstrated the synergistic effects of PPARγ ligands and ATRA on the differentiation of NB4 cells. The individual signaling pathways of RAR/RXR and PPARγ/RXR may have synergistically transduced signals for differentiation in NB4 cells. 9-*cis* RA, mono-*cis* isomers of retinoids, binds to RXR receptors in addition to RAR receptors and induces differentiation in HL-60 cells (Kizaki *et al.* 1993; Sakashita *et al.* 1993). However, 9-*cis* RA was clinically less effective for remission APL compared with ATRA. We did not perform experiments on the synergic effects of 9-*cis* RA with PPARγ ligands instead of ATRA in this study. Indeed, the duration of cell treatments being between 2 and 4 days, ATRA could be, at least partially, converted into 9-*cis* RA and 13-*cis* RA. In this case, the pathway of PPARγ/RXR may have induced differentiation by the synergic effects of 9-*cis* RA and PPARγ ligands. Further investigation will be needed to clarify this point.

In order to determine whether AD4833 or PGJ2 in fact binds PPARγ in NB4 cells, we examined the effects on differentiation using PPARγ or RXR antagonists. GW9662 and BADGE, both of which are specific PPARγ antagonists, significantly suppressed the differentiation of NB4 cells induced by PPARγ ligand and ATRA. The inhibitory effect of GW9662 was stronger than that of BADGE at the same concentration. Recently, Fehlberg *et al.* reported that high concentrations of BADGE induced apoptosis in tumor cells independently of PPARγ (Fehlberg *et al.* 2002). In our study, NB4 cells did not show apoptosis because we used a low concentration of agonist (data not shown). HX531 is an RXR antagonist but acts also as a potential inhibitor of PPARγ/RXR in an *in vitro* transactivation assay and to prevent triglyceride accumulation in 3T3L1 adipocytes (Yamauchi *et al.* 2001). HX531 significantly inhibited the differentiation of NB4 cells induced by PPARγ ligand and ATRA. Both PPARγ and RXR antagonists suppressed this differentiation, indicating that AD4833 and PGJ2 act on the cells via PPARγ/RXR receptor.

With regard to the effects of PPARγ ligands on the accumulation of lipid in the cytoplasm, several studies using rosiglitazone have found that PPARγ may promote macrophage lipid accumulation (Nagy *et al.* 1998; Tontonoz *et al.* 1998; Chawla *et al.* 2001). Recently, the opposite theory was proposed, namely that PPARγ activation by rosiglitazone is not related to lipid accumulation in macrophages (Chinetti *et al.* 2001; Moore *et al.* 2001; Vosper *et al.* 2001). Our findings were consistent with the former theory, that is, lipid droplets accumulated during differentiation in NB4 cells treated with PPARγ ligand and ATRA. The triacylglycerol levels in PPARγ ligand- and ATRA-treated cells were obviously higher than that in cells treated with ATRA alone (Fig. 6b). These findings suggest that PPARγ accelerated the formation of lipid droplets by upregulating gene expression related to lipogenesis in NB4 cells. We examined the enzyme activity of glycerol-3-phosphate dehydrogenase (GPDH; EC 1.1.1.8), and the expression of CD36 (scavenger receptor-class B, fatty acid translocase). However, there was no difference in the enzyme activity or protein expression between PPARγ ligand and ATRA-treated and untreated cells. CD36 expression was not detected by fluorescence activated cell sorting analysis in either untreated or treated cells (data not shown). On the other hand, expression of aP2 mRNA in NB4 cells was upregulated by PPARγ ligand treatments (Fig. 4).

Furthermore, to elucidate the features of lipogenesis during differentiation, we examined the incorporation of fluorescent fatty acids in the cytoplasm. The fluorescent analogue was rapidly converted to triacylglycerols and targeted to the lipid droplets in NB4 cells treated with PPARγ ligand and ATRA. Large lipid droplets from adipocytes, rich in triacylglycerols, are retained within the cells as a source of fatty acids for mitochondrial and peroxisomal oxidation to produce energy (Brasaemle *et al.* 1997). However, almost all other mammalian tissues examined contain small lipid droplets, which are less well characterized (Atshaves *et al.* 1998; Murphy & Vance 1999; Sparrow *et al.* 1999). Burns *et al.* reported that human neutrophils

take up much more fatty acid than lymphocytes primarily because they synthesize much larger quantities of triacylglycerols, a fatty acid storage form (Burns *et al.* 1976). It is postulated that lipid droplets may represent the storage form for free fatty acids which may be utilized for membrane synthesis during phagocytosis (Elsbach 1964; Elsbach & Farrow 1969; Lutas & Zucker-Franklin 1977). In these theories, the differentiation of phagocytes is accompanied by lipid droplet accumulation. We also examined the biosynthesis of triacylglycerols using fluorescent fatty acid. The results demonstrated that the rate of triacylglycerol synthesis is more than twofold greater in differentiated cells. From the results of triacylglycerol enzyme activity assays, we suggest that triacylglycerols are synthesized from glycerol but not dihydroxyacetone phosphate in PPARγ ligand- and ATRA-treated cells. In adipocytes, thiazolidinediones markedly induce glycerol kinase gene expression and stimulate the incorporation of glycerol rather than glucose into triacylglycerol (Guan *et al.* 2002). In the synthesis of glycerolipids, it is well established that glycerol has to be phosphorylated to glycerol-3-phosphate before acylation occurs. However, in the microsomal fraction of heart, liver, kidney, skeletal muscle and brain tissues, direct acylation of glycerol becomes more prominent when exogenous glycerol levels become elevated (Lee *et al.* 2001). Both of those reports are in accord with our conclusion that glycerol was used as substrate in triacylglycerol synthesis. Further investigations will be required to determine the relationship between differentiation and the accumulation of lipid droplets in acute myeloid leukemia treated with PPARγ ligands and ATRA.

Acknowledgement

We thank the Takeda Pharmaceutical Company (Tokyo, Japan) for providing AD4833.

References

Asou, H., Verbeek, W., Williamson, E. *et al.* 1999. Growth inhibition of myeloid leukemia cells by troglitazone, a ligand for peroxisome proliferator activated receptor γ, and retinoids. *Int. J. Oncol.* **15**, 1027–1031.

Atshaves, B. P., Foxworth, W. B., Frolov, A. *et al.* 1998. Cellular differentiation and I-FABP protein expression modulate fatty acid uptake and diffusion. *Am. J. Physiol.* **274**, C633–C644.

Boehm, M. F., Zhang, L., Zhi, L. *et al.* 1995. Design and synthesis of potent retinoid X receptor selective ligands that induce apoptosis in leukemia cells. *J. Med. Chem.* **38**, 3146–3155.

Brasaemle, D. L., Barber, T., Wolins, N. E., Serrero, G., Blanchette-Mackie, E. J. & Londos, C. 1997. Adipose differentiation-related protein is an ubiquitously expressed lipid storage droplet-associated protein. *J. Lipid Res.* **38**, 2249–2263.

Breitman, T. R., Selonick, S. E. & Collins, S. J. 1980. Induction of differentiation of the human promyelocytic leukemia cell line (HL-60) by retinoic acid. *Proc. Natl Acad. Sci. USA* **77**, 2936–2940.

Burns, C. P., Welshman, I. R. & Spector, A. A. 1976. Differences in free fatty acid and glucose metabolism of human blood neutrophils and lymphocytes. *Blood* **47**, 431–437.

Chawla, A., Barak, Y., Nagy, L., Liao, D., Tontonoz, P. & Evans, R. M. 2001. PPAR-γ dependent and independent effects on macrophage-gene expression in lipid metabolism and inflammation. *Nat. Med.* **7**, 48–52.

Chawla, A., Schwarz, E. J., Dimaculangan, D. D. & Lazar, M. A. 1994. Peroxisome proliferator-activated receptor (PPAR) γ: adipose-predominant expression and induction early in adipocyte differentiation. *Endocrinology* **135**, 798–800.

Chinetti, G., Lestavel, S., Bocher, V. *et al.* 2001. PPAR-α and PPAR-γ activators induce cholesterol removal from human macrophage foam cells through stimulation of the ABCA1 pathway. *Nat. Med.* **7**, 53–58.

Cornic, M., Delva, L., Guidez, F., Balitrand, N., Degos, L. & Chomienne, C. 1992. Induction of retinoic acid-binding protein in normal and malignant human myeloid cells by retinoic acid in acute promyelocytic leukemia patients. *Cancer Res.* **52**, 3329–3334.

Degos, L. 1992. Retinoic acid in acute promyelocytic leukemia: a model for differentiation therapy. *Curr. Opin. Oncol.* **4**, 45–52.

Ebisawa, M., Umemiya, H., Ohta, K. *et al.* 1999. Retinoid X receptor-antagonistic diazepinylbenzoic acids. *Chem. Pharm. Bull. (Tokyo)* **47**, 1778–1786.

Elsbach, P. 1964. Comparison of Uptake of Palmitic, Stearic, Oleic and Linoleic Acid by Polymorphonuclear Leukocytes. *Biochim. Biophys. Acta* **84**, 8–17.

Elsbach, P. & Farrow, S. 1969. Cellular triglyceride as a source of fatty acid for lecithin synthesis during phagocytosis. *Biochim. Biophys. Acta* **176**, 438–441.

Fehlberg, S., Trautwein, S., Goke, A. & Goke, R. 2002. Bisphenol A diglycidyl ether induces apoptosis in tumour cells independently of peroxisome proliferator-activated receptor-γ, in caspase-dependent and -independent manners. *Biochem. J.* **362**, 573–578.

Forman, B. M., Tontonoz, P., Chen, J., Brun, R. P., Spiegelman, B. M. & Evans, R. M. 1995. 15-Deoxy-Δ 12, 14-prostaglandin J2 is a ligand for the adipocyte determination factor PPAR γ. *Cell* **83**, 803–812.

Gearing, K. L., Gottlicher, M., Teboul, M., Widmark, E. & Gustafsson, J. A. 1993. Interaction of the peroxisome-proliferator-activated receptor and retinoid X receptor. *Proc. Natl Acad. Sci. USA* **90**, 1440–1444.

Greenspan, P., Mayer, E. P. & Fowler, S. D. 1985. Nile red: a selective fluorescent stain for intracellular lipid droplets. *J. Cell Biol.* **100**, 965–973.

Guan, H. P., Li, Y., Jensen, M. V., Newgard, C. B., Steppan, C. M. & Lazar, M. A. 2002. A futile metabolic cycle activated in adipocytes by antidiabetic agents. *Nat. Med.* **8**, 1122–1128.

Hirase, N., Yanase, T., Mu, Y. *et al.* 1999. Thiazolidinedione induces apoptosis and monocytic differentiation in the promyelocytic leukemia cell line HL60. *Oncology* **57** (Suppl. 2), 17–26.

Hu, Z. B., Ma, W., Uphoff, C. C., Lanotte, M. & Drexler, H. G. 1993. Modulation of gene expression in the acute promyelocytic leukemia cell line NB4. *Leukemia* **7**, 1817–1823.

Huang, M. E. Ye, Y. C., Chen, S. R. *et al.* 1988. Use of all-trans retinoic acid in the treatment of acute promyelocytic leukemia. *Blood* **72**, 567–572.

Kizaki, M., Ikeda, Y., Tanosaki, R. *et al.* 1993. Effects of novel retinoic acid compound, 9-cis-retinoic acid, on proliferation, differentiation, and expression of retinoic acid receptor-α and retinoid X receptor-α RNA by HL-60 cells. *Blood* **82**, 3592–3599.

Kliewer, S. A., Umesono, K., Mangelsdorf, D. J. & Evans, R. M. 1992a. Retinoid X receptor interacts with nuclear receptors in retinoic acid, thyroid hormone and vitamin D3 signalling. *Nature* **355**, 446–449.

Kliewer, S. A., Umesono, K., Noonan, D. J., Heyman, R. A. & Evans, R. M. 1992b. Convergence of 9-cis retinoic acid and peroxisome proliferator signalling pathways through heterodimer formation of their receptors. *Nature* **358**, 771–774.

Lee, D. P., Deonarine, A. S., Kienetz, M. *et al.* 2001. A novel pathway for lipid biosynthesis: the direct acylation of glycerol. *J. Lipid Res.* **42**, 1979–1986.

Lehmann, J. M., Moore, L. B., Smith-Oliver, T. A., Wilkison, W. O., Willson, T. M. & Kliewer, S. A. 1995. An antidiabetic thiazolidinedione is a high affinity ligand for peroxisome proliferator-activated receptor γ (PPAR γ). *J. Biol. Chem.* **270**, 12 953–12 956.

Lutas, E. M. & Zucker-Franklin, D. 1977. Formation of lipid inclusions in normal human leukocytes. *Blood* **49**, 309–320.

Moore, K. J., Rosen, E. D., Fitzgerald, M. L. *et al.* 2001. The role of PPAR-γ in macrophage differentiation and cholesterol uptake. *Nat. Med.* **7**, 41–47.

Mueller, E., Sarraf, P., Tontonoz, P. *et al.* 1998. Terminal differentiation of human breast cancer through PPAR γ. *Mol. Cell* **1**, 465–470.

Murphy, D. J. & Vance, J. 1999. Mechanisms of lipid-body formation. *Trends Biochem. Sci.* **24**, 109–115.

Nagy, L., Tontonoz, P., Alvarez, J. G., Chen, H. & Evans, R. M. 1998. Oxidized LDL regulates macrophage gene expression through ligand activation of PPAR γ. *Cell* **93**, 229–240.

Ohta, K., Kawachi, E., Inoue, N. *et al.* 2000. Retinoidal pyrimidinecarboxylic acids. Unexpected diaza-substituent effects in retinobenzoic acids. *Chem. Pharm. Bull. (Tokyo)* **48**, 1504–1513.

Rosen, E. D., Sarraf, P., Troy, A. E. *et al.* 1999. PPAR γ is required for the differentiation of adipose tissue in vivo and in vitro. *Mol. Cell* **4**, 611–617.

Sakashita, A., Kizaki, M., Pakkala, S. *et al.* 1993. 9-cis-retinoic acid: effects on normal and leukemic hematopoiesis in vitro. *Blood* **81**, 1009–1016.

Schulman, I. G., Shao, G. & Heyman, R. A. 1998. Transactivation by retinoid X receptor-peroxisome proliferator-activated receptor γ (PPAR γ) heterodimers: intermolecular synergy requires only the PPAR γ hormone-dependent activation function. *Mol. Cell Biol.* **18**, 3483–3494.

Sparrow, C. P., Patel, S., Baffic, J. *et al.* 1999. A fluorescent cholesterol analog traces cholesterol absorption in hamsters and is esterified in vivo and in vitro. *J. Lipid. Res.* **40**, 1747–1757.

Thuillier, P., Baillie, R., Sha, X. & Clarke, S. D. 1998. Cytosolic and nuclear distribution of PPAR γ 2 in differentiating 3T3-L1 preadipocytes. *J. Lipid Res.* **39**, 2329–2338.

Tontonoz, P., Hu, E. & Spiegelman, B. M. 1994. Stimulation of adipogenesis in fibroblasts by PPAR γ 2, a lipid-activated transcription factor. *Cell* **79**, 1147–1156.

Tontonoz, P., Nagy, L., Alvarez, J. G., Thomazy, V. A. & Evans, R. M. 1998. PPAR γ promotes monocyte/macrophage differentiation and uptake of oxidized LDL. *Cell* **93**, 241–252.

Vosper, H., Patel, L., Graham, T. L. *et al.* 2001. The peroxisome proliferator-activated receptor δ promotes lipid accumulation in human macrophages. *J. Biol. Chem.* **276**, 44 258–44 265.

Westin, S., Kurokawa, R., Nolte, R. T. *et al.* 1998. Interactions controlling the assembly of nuclear-receptor heterodimers and co-activators. *Nature* **395**, 199–202.

Willson, T. M., Lambert, M. H. & Kliewer, S. A. 2001. Peroxisome proliferator-activated receptor γ and metabolic disease. *Annu. Rev. Biochem.* **70**, 341–367.

Wright, H. M., Clish, C. B., Mikami, T. *et al.* 2000. A synthetic antagonist for the peroxisome proliferator-activated receptor γ inhibits adipocyte differentiation. *J. Biol. Chem.* **275**, 1873–1877.

Yamauchi, T., Waki, H., Kamon, J. *et al.* 2001. Inhibition of RXR and PPAR γ ameliorates diet-induced obesity and type 2 diabetes. *J. Clin. Invest* **108**, 1001–1013.

Yasugi, E., Uemura, I., Kumagai, T., Nishikawa, Y., Yasugi, S. & Yuo, A. 2002. Disruption of mitochondria is an early event during dolichyl monophosphate-induced apoptosis in U937 cells. *Zool. Sci.* **19**, 7–13.

Zilberfarb, V., Siquier, K., Strosberg, A. D. & Issad, T. 2001. Effect of dexamethasone on adipocyte differentiation markers and tumour necrosis factor-α expression in human PAZ6 cells. *Diabetologia* **44**, 377–386.

International Journal of
HEMATOLOGY

Identification of Human Neutrophils during Experimentally Induced Inflammation in Mice with Transplanted CD34$^+$ Cells from Human Umbilical Cord Blood

Masaru Doshi, Makoto Koyanagi, Masako Nakahara, Koichi Saeki, Kumiko Saeki, Akira Yuo

Department of Hematology, Research Institute, International Medical Center of Japan, Tokyo, Japan

Received February 10, 2006; received in revised form June 1, 2006; accepted June 22, 2006

Abstract

Nonobese diabetic/severe combined immunodeficiency/γ chain^{null} (NOG) mice are excellent recipients for xenotransplantation and have been especially valuable for the evaluation of human hematopoietic stem cell (HSC) activities. Because human hematopoietic cells that developed in this mouse were mainly lymphoid cells and not myeloid cells, mature human myeloid cells such as neutrophils were hardly detectable in peripheral blood. We demonstrated that human neutrophils accumulated by means of a zymosan-induced air pouch inflammation technique could be identified with a fluorescence-activated cell sorter in NOG mice with transplanted CD34$^+$ cells from human umbilical cord blood, which were putative hematopoietic progenitor cells including HSC. Our results indicate that human neutrophils with a chemotactic capacity can develop from human hematopoietic progenitor cells in vivo, suggesting that our system may be a useful tool for the evaluation of human HSC activities.

Int J Hematol. 2006:84:231-237. doi: 10.1532/IJH97.06040

Key words: NOG mice; Transplantation; Human hematopoietic stem cells; Human neutrophils; Chemotaxis

1. Introduction

Hematopoietic stem cells (HSC) have been defined to possess both the ability to self-renew and the capacity to differentiate into full lineages of hematopoietic cells [1], capabilities that have been evaluated by the transplantation of human cells into experimental animals. Nonobese diabetic/severe combined immunodeficiency (NOD/SCID) mice have widely been used as recipients in xenotransplantation to evaluate the abilities of human HSC, although the engraftment rate of human hematopoietic cells in these mice has been low [2].

NOD/SCID/γ chain (γc)^{null} (NOG) mice, an NOD/SCID mouse strain that lacks the interleukin 2 receptor γc, were recently established to improve the engraftment efficiency of the conventional NOD/SCID mouse, which possesses natural killer cell activity [3]. Several studies have demonstrated that human hematopoietic cells develop in hematopoietic tissue or the peripheral blood of NOG mice that have received transplants of human hematopoietic progenitor cells, such as umbilical cord blood (CB) and bone marrow CD34$^+$ cells containing HSC [3-6]. However, because the human hematopoietic cells that developed in these mice were mainly lymphoid cells and not myeloid cells [4-6], mature human myeloid cells such as neutrophils were hardly detectable in the peripheral blood of the mice that had received such transplants. Therefore, no study has definitely identified human neutrophils in mice with transplanted human hematopoietic progenitor cells.

Human neutrophils, a primary constituent of peripheral blood leukocytes, play an important role during host defense against invading microorganisms [7]. The decreased numbers of neutrophils or attenuated function of neutrophils results in serious infections in several pathologic situations, such as congenital leukocyte function deficiencies or myelosuppression caused by chemotherapy [8,9]. The microbicidal functions of neutrophils are executed via total harmonization of all their specific functions, such as chemotaxis, adhesion, phagocytosis, and respiratory burst activity [10]. Several conventional methods are available to evaluate these effector functions of human neutrophils in vitro [11]. In addition, some functions, such as chemotaxis,

Correspondence and reprint requests: Akira Yuo, MD, PhD, Department of Hematology, Research Institute, International Medical Center of Japan, 1-21-1, Toyama, Shinjuku-ku, Tokyo 162-8655, Japan; 81-3-3202-7181; fax: 81-3-3207-1038 (e-mail: yuoakira@ri.imcj.go.jp).

can be evaluated in vivo by using the acute-inflammation model in mice [12].

Acute inflammation is induced by the injection of zymosan into a dorsal air pouch created in a mouse and the subsequent accumulation of a large number of murine neutrophils into the air pouch [13,14]. Consequently, highly purified murine neutrophils with a sufficient capacity to migrate from other sites, such as the peripheral blood, into inflammatory sites can be isolated from mice by means of this inflammation model. Our objective was to investigate whether the zymosan-injection air pouch methodology can be used in immunodeficient mice with transplanted human HSC to elicit neutrophil migration and inflammation. This methodology gives us the opportunity to evaluate not only human neutrophil production but also critical functions of engrafted human neutrophils.

2. Materials and Methods

2.1. Animals

The experimental protocol was approved by the Committee of Animal Care and Experiments of the Research Institute of the International Medical Center of Japan (IMCJ) (protocol no. 17-Tg-7). NOG mice were purchased from the Central Institute of Experimental Animals (CIEA) (Kanagawa, Japan). All mice were kept under specific pathogen-free conditions at the animal laboratory of the Research Institute of IMCJ in accordance with CIEA guidelines.

2.2. Transplantation of Human CB CD34$^+$ Cells into Mice

Nine-week-old female NOG mice were sublethally irradiated with 2 Gy via an MBR1520-3 x-ray source (Hitachi Medical, Tokyo, Japan). After 24 hours, mice received intravenous transplants of 1.8×10^5 human CB CD34$^+$ cells (AllCells, Berkeley, CA, USA) or vehicle (saline). The purity and viability of the CB CD34$^+$ cells were greater than 95%.

2.3. Zymosan-Induced Air Pouch Inflammation

Six, 8, or 10 weeks after the transplantation of human CB CD34$^+$ cells, a subcutaneous air pouch was formed on the back of NOG mice, as has been described previously [13,14]. Five hundred microliters of zymosan solution (1 mg/mL in saline) was injected into the air pouch. Sixteen hours after zymosan injection, mice were decapitated under diethyl ether anesthesia, and the air pouch was washed with 1 mL of ice-cold phosphate-buffered saline (PBS) to obtain accumulated leukocytes.

2.4. Determination of Superoxide Release

Superoxide release stimulated by phorbol myristate acetate was assayed by the superoxide dismutase–inhibitable reduction of ferricytochrome c, which was monitored continuously in a Hitachi 556 double-wavelength spectrophotometer (Hitachi High-Technologies, Tokyo, Japan) equipped with a thermostatted cuvette holder (37°C), as described previously [11].

2.5. Preparation of Neutrophils from Human Peripheral Blood

Granulocytes and mononuclear cells were prepared from healthy adult donors as described previously [11] by using dextran (Nacalai Tesque, Kyoto, Japan) sedimentation, centrifugation with a separating solution (Lymphoprep; Axis-Shield, Oslo, Norway), and hypotonic lysis of the contaminating erythrocytes. Neutrophils constituted greater than 90% of the granulocyte fractions, and the remaining cells were eosinophils. Mononuclear cell fractions consisted of 20% monocytes and 80% lymphocytes. Both cell fractions were suspended in PBS containing 5% fetal calf serum (FCS).

2.6. Preparation of Murine Bone Marrow and Spleen Leukocytes

Bone marrow cells were harvested from the mice by flushing the femurs with ice-cold Hanks balanced salt solution (HBSS). Spleens were harvested from the mice and minced in ice-cold HBSS. The resulting cell suspensions were filtered through a nylon mesh, and contaminating erythrocytes were eliminated by hypotonic lysis. The cells were then washed once and suspended in PBS containing 5% FCS.

2.7. Determination of Cell Surface Antigens by Fluorescence-Activated Cell Sorting

All suspensions of single cells were stained with the appropriate antibodies and analyzed by fluorescence-activated cell sorting (FACS) with a FACSCalibur flow cytometer (BD Biosciences, San Jose, CA, USA). Cells were incubated with monoclonal antibodies for 30 minutes on ice in PBS containing 5% FCS. Nonspecific binding to cells bearing Fcγ receptors was blocked with a rat antimouse CD16/CD32 monoclonal antibody (BD Biosciences). The following monoclonal antibodies were used in this flow cytometric study: fluorescein isothiocyanate (FITC)-conjugated rat antimouse Ly-6G and Ly-6C antibody (Gr-1 antibody) (BD Biosciences), phycoerythrin (PE)-conjugated mouse antihuman CD45 (BD Biosciences), PE-conjugated mouse antihuman CD10 (BD Biosciences), FITC-conjugated mouse antihuman CD66b (Beckman Coulter, Miami, FL, USA), and each isotype as a control. Antimouse Gr-1 antibody, which reacts selectively with murine neutrophils, does not cross-react with human hematopoietic cells, including neutrophils, and antihuman CD45, CD10, and CD66b antibodies, which react selectively with human neutrophils, do not cross-react with murine neutrophils.

2.8. Immunocytochemical Study

Cells collected from air pouches were washed with PBS and fixed on glass slides by means of a Cytospin apparatus (Cytospin 2; Shandon, Pittsburgh, PA, USA). After further fixation with acetone/methanol solution (1:3), immunostaining was performed as described previously [15] by using FITC-conjugated antihuman CD16b monoclonal antibody (Beckman Coulter) or antihuman CD45 monoclonal

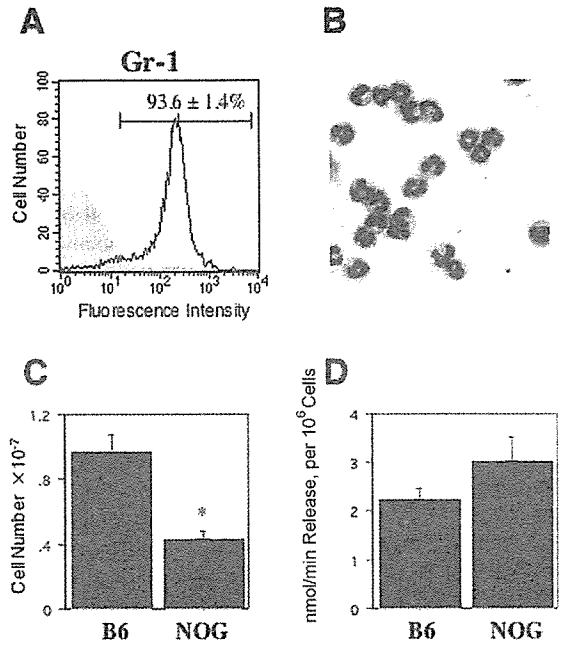

Figure 1. Air pouch inflammatory model in nonobese diabetic/severe combined immunodeficiency/γ chain^{null} (NOG) mice. Zymosan suspended in saline (0.5 mg/mouse) was injected into the air pouch of NOG mice to induce inflammation. The pouch was washed with phosphate-buffered saline 16 hours after zymosan injection to obtain accumulated leukocytes. A, Fluorescence-activated cell-sorting analysis of the expression of the granulocyte-specific antigen Gr-1 was carried out with leukocytes from the air pouch of NOG mice (n = 3). B, Morphology of the leukocytes in the air pouch of NOG mice. After fixation to glass slides, cells were stained with Wright-Giemsa solution and examined by light microscopy. C, The number of leukocytes in the air pouch was determined in B6 and NOG mice. D, The respiratory burst activities of granulocytes in the air pouch in B6 and NOG mice. Superoxide (O_2^-) release stimulated by 100 ng/mL phorbol myristate acetate was determined by the reduction of cytochrome *c* and is expressed as nmol/minute per 10^6 cells. Data for (C) and (D) are expressed as the mean ± SE (n = 6), and statistical analysis was performed by means of an unpaired Student *t* test. **P* < .05, NOG versus B6 mice.

antibody (BD Biosciences). For the control, an isotype antibody reaction was performed by using FITC-conjugated immunoglobulin M (IgM) κ (ICN Biomedicals, Aurora, OH, USA) and IgG1 κ (BD Biosciences) for the anti-CD16b and anti-CD45 antibody reactions, respectively. The second antibody reaction was performed by using Alexa Fluor 488 goat antimouse IgM (Invitrogen, Carlsbad, CA, USA) and Alexa Fluor 488 goat antimouse IgG (Invitrogen) for the anti-CD16b and anti-CD45 antibody reactions, respectively.

2.9. Morphologic Observation

Cells were fixed on glass slides with a Cytospin 2 apparatus, stained with Wright-Giemsa solution (Muto Pure Chemical, Tokyo, Japan), and then observed with a light microscope (Olympus Optical, Tokyo, Japan).

2.10. Statistical Analysis

Statistical analysis was performed by means of the unpaired Student *t* test and the StatView software package (version 5.0; SAS Institute/Abacus Concepts, Berkeley, CA, USA).

3. Results

3.1. Zymosan-Induced Air Pouch Inflammation in NOG Mice

The leukocytes that accumulate by zymosan-induced air pouch inflammation in normal mice are known to be predominantly neutrophils, along with small numbers of monocytes and lymphocytes (data for normal B6 mice are not shown) [13,14]. In the present study, we first investigated whether zymosan-induced accumulation of mature murine neutrophils into the air pouch also occurs in NOG mice.

As has been observed with this inflammatory model in normal mice, the leukocytes that accumulated in the air pouch after zymosan injection in NOG mice were predominantly neutrophils. This result was established by detecting the expression of a specific surface antigen of mouse neutrophils, Gr-1, as well as the typical morphologic characteristics obtained via Wright-Giemsa staining (Figures 1A and 1B). Both the FACS analysis of the Gr-1 antigen and the morphologic evaluation indicated that greater than 90% of the accumulated leukocytes were neutrophils. In the NOG mice lacking lymphocytes, the remaining leukocytes (<10%) were monocytes (data not shown).

These results indicate that the migration of neutrophils toward inflammatory sites occurs almost normally in NOG mice, suggesting that the neutrophils of NOG mice have a normal chemotactic function. The number of leukocytes in the air pouch of NOG mice, however, was significantly lower ($P < .05$) than that of B6 mice (Figure 1C). On the other hand, the respiratory burst activity, another important function of neutrophils, was normal, because agonist-induced superoxide release from the leukocytes in the air pouch of NOG mice was equivalent to that of B6 mice (Figure 1D).

3.2. Engraftment of Human CB CD34⁺ Cells in NOG Mice

We next transplanted human CB CD34⁺ cells into recipient NOG mice. After being sublethally irradiated, NOG mice received intravenous transplants of human CB CD34⁺ cells. Six weeks after transplantation, leukocytes in the bone marrow and spleen were analyzed for the expression of the human panleukocyte marker, CD45 (Figure 2). In these hematopoietic organs, approximately 90% of the cells expressed human CD45 antigen, both at 6 weeks and at 8 weeks after the transplantation of human CB CD34⁺ cells (Figure 2). These findings indicate the highly effective engraftment of human hematopoietic cells in this immunodeficient mouse, and the efficiency of engraftment obtained in

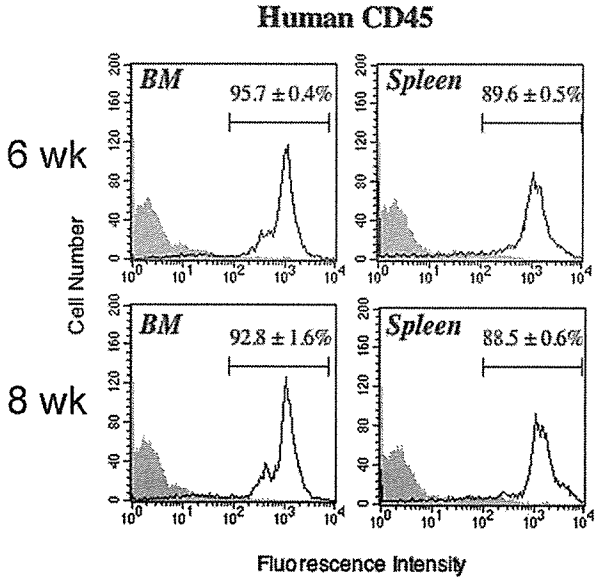

Figure 2. Engraftment of human cord blood CD34$^+$ cells in nonobese diabetic/severe combined immunodeficiency/γ chain^{null} (NOG) mice. CD34$^+$ cells from human umbilical cord blood (1.8×10^5 cells/mouse) were transplanted into NOG mice intravenously. Bone marrow (BM) and spleen leukocytes were obtained at 6 and 8 weeks after transplantation as described in "Materials and Methods." Cell surface expression of human CD45 was determined by fluorescence-activated cell-sorting analysis. Data are expressed as the mean ± SE (n = 3).

this study was equivalent to or better than the results described in previous reports [3,4].

We then evaluated whether CD45$^+$ human hematopoietic cells appear in the air pouch of NOG mice that had received transplants of human CB CD34$^+$ cells. As is shown in Figure 3 (upper panel), more than 90% of the leukocytes in the air pouch of NOG mice infused with vehicle alone were Gr-1$^+$ murine neutrophils, and there were no human CD45$^+$ leukocytes. In contrast, a significant level (approximately 10%) of human CD45$^+$ cells in the air pouch was present in NOG mice that had received transplants of human CB CD34$^+$ cells, and there was a concomitant decrease in the percentage of Gr-1$^+$ murine neutrophils. We observed these findings at both 6 weeks and 8 weeks after transplantation of human CB CD34$^+$ cells, although the human CD45$^+$ cells in the air pouch had decreased at 8 weeks for an unknown reason.

3.3. Identification of Human Neutrophils Accumulated by Zymosan-Induced Air Pouch Inflammation in Mice with Transplanted Human CB CD34$^+$ Cells

Because most of the leukocytes in zymosan-induced air pouch inflammation were neutrophils, the human CD45$^+$ leukocytes in Figure 3 were considered human neutrophils that had differentiated in vivo in the NOG mice. To further confirm this hypothesis, we performed FACS analysis with monoclonal antibodies that specifically recognize mature human neutrophils. We selected 2 neutrophil-specific cell surface molecules, CD10 and CD66b. CD10, well known as a common acute lymphoblastic leukemia antigen [16], has been reported to be expressed in mature neutrophils [17-19], and CD66b is a specific cell surface antigen of human granulocytes [20].

Before the transplantation experiments with NOG mice, we performed several experiments with normal human neutrophils and mononuclear leukocytes to establish experimental conditions for the 2-color flow cytometric analysis of CD10 and CD66b. As is shown in Figure 4 (upper panel), we successfully performed 2-color analysis with a granulocyte fraction isolated from a healthy donor. The granulocyte fraction contained 96.5% CD66b$^+$ granulocytes, which consisted of 86.3% CD10$^+$ neutrophils and 10.2% other CD10$^-$ granulocytes, probably eosinophils. This granulocyte fraction contained more than 98% CD45$^+$ cells (data not shown). In contrast, the cells in mononuclear cell fractions were negative for both CD66b and CD10.

Using this analytical condition, we then performed a 2-color flow cytometric analysis of the leukocytes that had

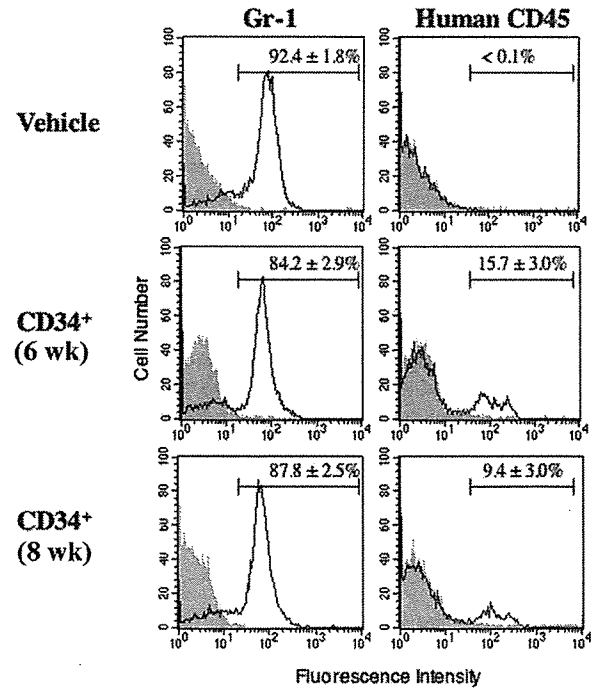

Figure 3. Identification of human leukocytes in the air pouch of nonobese diabetic/severe combined immunodeficiency/γ chain^{null} (NOG) mice. CD34$^+$ cells from human umbilical cord blood (1.8×10^5 cells/mouse) (CD34$^+$) or saline (vehicle) was transplanted into NOG mice intravenously. Zymosan was suspended in saline (0.5 mg/mouse) and injected into the air pouch to induce inflammation by 6 or 8 weeks after transplantation. The pouch was washed with phosphate-buffered saline 16 hours after zymosan injection to obtain accumulated leukocytes. Cell surface expression of murine Gr-1 and human CD45 was determined by fluorescence-activated cell-sorting analysis. Data are expressed as the mean ± SE (n = 3).

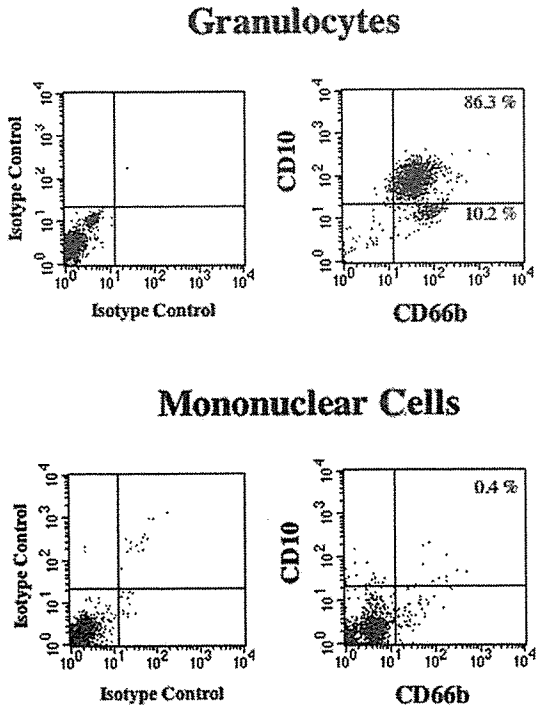

Figure 4. Two-color fluorescence-activated cell-sorting (FACS) analysis of CD10 and CD66b in human peripheral blood leukocytes. Human granulocytes and mononuclear cells were isolated as described in "Materials and Methods." Two-color FACS analysis of the cell surface expression of human CD10 and CD66b was performed with each isotype antibody as a control.

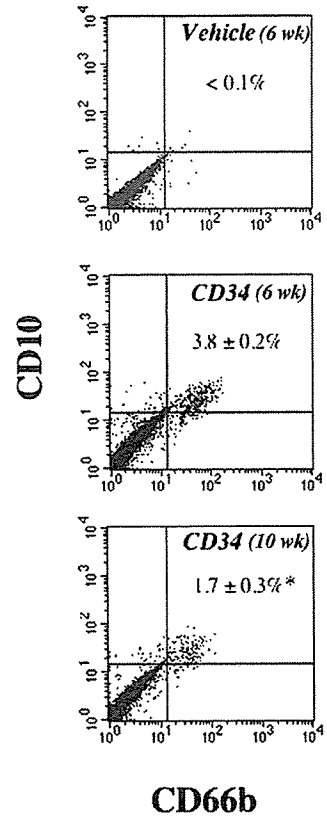

Figure 5. Two-color fluorescence-activated cell-sorting (FACS) analysis of CD10 and CD66b in leukocytes in the zymosan-induced air pouch in nonobese diabetic/severe combined immunodeficiency/γ chain^{null} (NOG) mice with transplanted human umbilical cord blood (CB) CD34$^+$ cells. Human CB CD34$^+$ cells (1.8×10^5 cells/mouse) were transplanted into NOG mice intravenously. Zymosan suspended in saline (0.5 mg/mouse) was injected into the air pouch to induce inflammation at 6 or 10 weeks after transplantation (middle and lower panels). Sixteen hours after zymosan injection, the pouch was washed with phosphate-buffered saline to obtain accumulated leukocytes. Cell surface expression of human CD10 and CD66b was determined by FACS analysis. As a negative control, leukocytes that had accumulated in the air pouch in NOG mice without CD34$^+$ cell transplantation were analyzed, and the results are shown in the top panel. Data are expressed as the mean ± SE (n = 3). Statistical analysis was performed by means of an unpaired Student *t* test. $^*P < .05$, 10 weeks versus 6 weeks.

accumulated in the air pouch after zymosan injection into mice with transplanted human CB CD34$^+$ cells. As is shown in Figure 5, double-positive (both CD10$^+$ and CD66b$^+$) human neutrophils were detected in the air pouch at both 6 weeks and 10 weeks after the transplantation of human CB CD34$^+$ cells. It is interesting that the double-positive human neutrophils in the air pouch had decreased by 10 weeks, compared with the numbers at 6 weeks. These data for double-positive human neutrophils in the air pouch almost corresponded to the data estimated from the numbers of human CD45$^+$ leukocytes in the air pouch (data not shown).

Finally, we used immunocytochemical staining to confirm that human neutrophils actually existed in the air pouch following zymosan injection into mice with transplanted human CB CD34$^+$ cells. As is shown in Figure 6, we were able to detect human CD45$^+$ cells with a neutrophil morphology in the leukocytes that had accumulated in the air pouch of mice with transplanted human CB CD34$^+$ cells. In contrast, human CD45$^+$ cells were not observed in the leukocytes that had accumulated in the air pouch of mice that had not undergone transplantation (data not shown). The presence of human neutrophils in the air pouch of mice with transplanted human CB CD34$^+$ cells was also confirmed with antihuman neutrophil-specific CD16b antibody (Figure 7).

Thus, using an in vivo inflammatory model, we have shown the functional engraftment of human neutrophils.

4. Discussion

Mature human neutrophils derived from human hematopoietic progenitor cells have not been identified in the peripheral blood of immunodeficient mice with transplanted human HSC, although HSC are considered to dif-

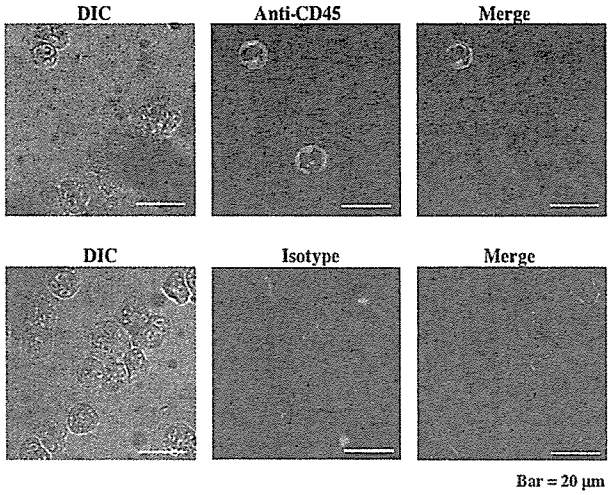

Figure 6. Immunocytochemical analysis of CD45 in leukocytes in the zymosan-induced air pouch in nonobese diabetic/severe combined immunodeficiency/γ chain^{null} (NOG) mice with transplanted CD34$^+$ cells from human umbilical cord blood (CB). Human CB CD34$^+$ cells (1.8×10^5 cells/mouse) were transplanted into NOG mice intravenously. Zymosan suspended in saline (0.5 mg/mouse) was injected into the air pouch to induce inflammation at 6 weeks after transplantation. The pouch was washed with phosphate-buffered saline 16 hours after zymosan injection to obtain accumulated leukocytes. Immunocytochemical analysis of human CD45 expression (top) was performed with isotype antibody as a control (bottom), and the staining pattern was observed with an inverted microscope. The left panels are difference interference contrast (DIC) images, the middle panels are the corresponding images obtained by fluorescence microscopy, and the right panels are combined images of the corresponding left and middle panels.

ferentiate into all hematopoietic cell lineages, including neutrophils. In the present study, we established a novel system to detect human neutrophils in NOG mice with transplanted human CB CD34$^+$ cells by using a model of experimentally induced inflammation and a 2-color FACS analysis that used 2 monoclonal antibodies specific for mature human neutrophils and/or granulocytes (Figure 5). In addition, the results obtained with our system, which selectively detects neutrophils that have migrated into the site of inflammation, indicated that the functional human neutrophils had developed from human hematopoietic progenitor cells in vivo.

Analysis of the cell surface antigens of leukocytes by FACS has been widely performed in many immunologic and hematologic studies because morphologic identification has not been capable of distinguishing lymphocyte subpopulations. In contrast, studies for specific cell surface markers of human neutrophils have been extremely limited, because human neutrophils are easily recognized by their morphology and there are no distinct subpopulations with the same morphology. However, to distinguish precisely between human and mouse neutrophils in chimeric mice with transplanted human hematopoietic progenitor cells requires determining specific cell surface antigens of human neutrophils. In the murine system, Gr-1 is a well-known granulocyte-specific cell surface marker and is known as a common epitope of Ly-6 subtypes in mice [21]. Stroncek et al reported that CD177, known as human neutrophil-specific antigen NB1, was a member of the Ly-6 gene superfamily and that it might be a human counterpart of Gr-1 [22]. However, the level of CD177 expression in human neutrophils is approximately 50% (unpublished data), suggesting that CD177 is not suitable for the complete identification of human neutrophils. In contrast, the present study clearly revealed that human neutrophils could be identified by a 2-color FACS analysis of 2 cell surface antigens, CD10 and CD66b, which are specific markers for granulocytes and/or neutrophils (Figure 4).

We found that neutrophil accumulation during zymosan-induced acute inflammation was reduced in NOG mice, compared with B6 mice (Figure 1C). Zymosan is known to activate the alternative pathway of complement and C5a formation [12], and inflammatory mediators, such as arachidonate metabolites, that are released from resident macrophages upon zymosan stimulation cause neutrophils to accumulate at the site of inflammation [23]. NOG mice have multiple immunologic defects in innate immunity, including a lack of macrophage function, complement-dependent hemolytic activity, and natural killer cell activity [3]. Therefore, the reduction of macrophage function and complement-

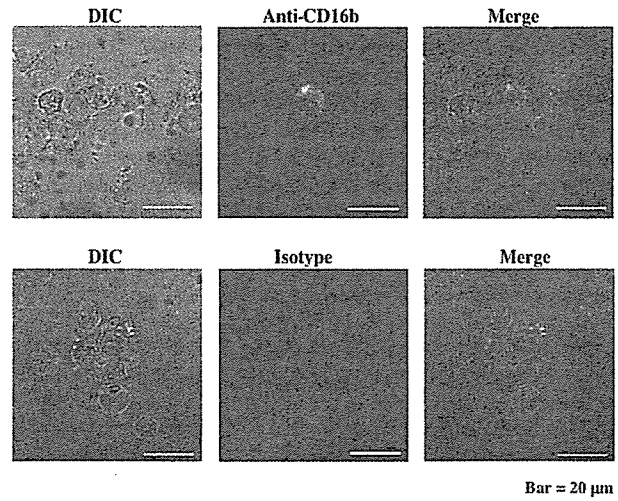

Figure 7. Immunocytochemical analysis of CD16b in leukocytes in the zymosan-induced air pouch in nonobese diabetic/severe combined immunodeficiency/γ chain^{null} (NOG) mice with transplanted CD34$^+$ cells from human umbilical cord blood (CB). Human CB CD34$^+$ cells (1.8×10^5 cells/mouse) were transplanted into NOG mice intravenously. Zymosan suspended in saline (0.5 mg/mouse) was injected into the air pouch to induce inflammation at 6 weeks after transplantation. The pouch was washed with phosphate-buffered saline 16 hours after zymosan injection to obtain accumulated leukocytes. Immunocytochemical analysis of human CD16b expression (top) was performed with isotype antibody as a control (bottom), and the staining pattern was observed with an inverted microscope. The left panels are difference interference contrast (DIC) images, the middle panels are the corresponding images obtained by fluorescence microscopy, and the right panels are combined images of the corresponding left and middle panels.

dependent hemolytic activity may account for the reduction of neutrophil accumulation during zymosan-induced acute inflammation in NOG mice. On the other hand, superoxide-producing capacity, another important function of neutrophils, was normal in NOG mice (Figure 1D). Therefore, the development and function of neutrophils are considered normal to some degree in NOG mice.

Previous studies have shown that engraftment of human $CD45^+$ cells in NOG mice is lymphocyte predominant and that engraftment increases gradually for 4 to 12 weeks following the transplantation of human CB $CD34^+$ cells [3,5,6]. On the other hand, we found that the engraftment of human neutrophils as estimated by our in vivo air pouch inflammatory model declined from 6 to 10 weeks after the transplantation of human $CD34^+$ cells (Figures 3 and 5). Although the exact reason for these different observations remains unclear, there are 2 possibilities: (1) extremely different life cycle and production kinetics for neutrophils and lymphocytes, or (2) the relatively normal development of murine neutrophils versus an almost complete lack of murine lymphocytes in NOG mice.

Investigators have recently concluded that human embryonic stem cells constitute a valuable resource for regenerative medicine because of their high capacity to differentiate into a broad range of cell types [24]. Consequently, many researchers have been vigorously studying such cells to establish culture conditions and techniques for the in vitro differentiation of human embryonic stem cells into hematopoietic stem or progenitor cells [25,26]. For clinical applications, however, both the differentiation and therapeutic potential of such cells should be investigated and evaluated in vivo, although performing such in vivo studies is not allowed in human beings. Therefore, our system may be useful as an in vivo system to evaluate the hematopoietic activities, particularly granulopoietic, of human hematopoietic progenitor cells derived from human embryonic stem cells.

Acknowledgment

This work was supported by a Sasakawa Scientific Research Grant from the Japan Science Society.

References

1. Osawa M, Hanada K, Hamada H, Nakauchi H. Long-term lymphohematopoietic reconstitution by a single CD34-low/negative hematopoietic stem cell. *Science.* 1996;273:242-245.
2. Greiner DL, Hesselton RA, Shultz LD. SCID mouse models of human stem cell engraftment. *Stem Cells.* 1998;16:166-177.
3. Ito M, Hiramatsu H, Kobayashi K, et al. NOD/SCID/γc^{null} mice: an excellent recipient mouse model for engraftment of human cells. *Blood.* 2002;100:3175-3182.
4. Matsumura T, Kametani Y, Ando K, et al. Functional $CD5^+$ B cells develop predominantly in the spleen of NOD/SCID/γc^{null} (NOG) mice transplanted either with human umbilical cord blood, bone marrow, or mobilized peripheral blood $CD34^+$ cells. *Exp Hematol.* 2003;31:789-797.
5. Kambe N, Hiramatsu H, Shimonaka M, et al. Development of both human connective tissue-type and mucosal-type mast cells in mice from hematopoietic stem cells with identical distribution pattern to human body. *Blood.* 2004;103:860-867.
6. Yahata T, Ando K, Nakamura Y, et al. Functional human T lymphocyte development from cord blood $CD34^+$ cells in nonobese diabetic/Shi-*scid*, IL-2 receptor γ null mice. *J Immunol.* 2002;169:204-209.
7. Witko-Sarsat V, Rieu P, Descamps-Latscha B, Lesavre P, Halbwachs-Mecarelli L. Neutrophils: molecules, functions and pathophysiological aspects. *Lab Invest.* 2002;80:617-653.
8. Johnston RB Jr. Clinical aspects of chronic granulomatous disease. *Curr Opin Hematol.* 2001;8:17-22.
9. Johnston EM, Crawford J. Hematopoietic growth factors in the reduction of chemotherapeutic toxicity. *Semin Oncol.* 1998;25:552-561.
10. Yuo A. Differentiation, apoptosis, and function of human immature and mature myeloid cells: intracellular signaling mechanism. *Int J Hematol.* 2001;73:438-452.
11. Yuo A, Kitagawa S, Ohsaka A, et al. Recombinant human granulocyte colony-stimulating factor as an activator of human granulocytes: potentiation of responses triggered by receptor-mediated agonists and stimulation of C3bi receptor expression and adherence. *Blood.* 1989;74:2144-2149.
12. Rao TS, Currie JL, Shaffer AF, Isakson PC. In vivo characterization of zymosan-induced mouse peritoneal inflammation. *J Pharmacol Exp Ther.* 1994;293:917-925.
13. Posadas I, Terencio MC, Guilltén I, Ferrándiz ML, Payá M, Alcaraz MJ. Co-regulation between cyclo-oxygenase-2 and inducible nitric oxide synthase expression in the time-course of murine inflammation. *Naunyn Schmiedebergs Arch Pharmacol.* 2000;361:98-106.
14. Doshi M, Watanabe S, Niimoto T, et al. Effect of dietary enrichment with n-3 polyunsaturated fatty acids (PUFA) or n-9 PUFA on arachidonate metabolism *in vivo* and experimentally induced inflammation in mice. *Biol Pharm Bull.* 2004;27:319-323.
15. Saeki K, Yasugi E, Okuma E, et al. Proteomic analysis on insulin signaling in human hematopoietic cells: identification of CLIC1 and SRp20 as novel downstream effectors of insulin. *Am J Physiol Endocrinol Metab.* 2005;289:E419-E428.
16. Uckun FM, Ledbetter JA. Immunobiologic differences between normal and leukemic human B-cell precursors. *Proc Natl Acad Sci U S A.* 1988;85:8603-8607.
17. Braun MP, Martin PJ, Ledbetter JA, Hansen JA. Granulocytes and cultured human fibroblasts express common acute lymphoblastic leukemia-associated antigens. *Blood.* 1983;61:718-725.
18. Cossman J, Neckers LM, Leonard WJ, Greene WC. Polymorphonuclear neutrophils express the common acute lymphoblastic leukemia antigen. *J Exp Med.* 1983;157:1064-1069.
19. Iwamoto I, Kimura A, Ochiai K, Yoshida S. Distribution of neutral endopeptidase activity in human blood leukocytes. *J Leukoc Biol.* 1991;49:116-125.
20. Zhao L, Xu S, Fjaertoft G, Pauksen K, Hakansson L, Venge P. An enzyme-linked immunosorbent assay for human carcinoembryonic antigen-related cell adhesion molecule 8, a biological marker of granulocyte activities in vivo. *J Immunol Methods.* 2004;293:207-214.
21. Fleming TJ, Fleming ML, Malek TR. Selective expression of Ly-6G on myeloid lineage cells in mouse bone marrow: RB6-8C5 mAb to granulocyte-differentiation antigen (Gr-1) detects members of the Ly-6 family. *J Immunol.* 1993;151:2399-2408.
22. Stroncek DF, Caruccio L, Bettinotti M. *CD177*: a member of the Ly-6 gene superfamily involved with neutrophil proliferation and polycythemia vera. *J Transl Med.* 2004;2:8.
23. Lefkowith JB. Essential fatty acid deficiency inhibits the in vivo generation of leukotriene B4 and suppresses levels of resident and elicited leukocytes in acute inflammation. *J Immunol.* 1988;140:228-233.
24. Thomson JA, Itskovitz-Eldor J, Shapiro SS, et al. Embryonic stem cell lines derived from human blastocyst. *Science.* 1998;282:1145-1147.
25. Vodyanik MA, Bork JA, Thomson JA, Slukvin II. Human embryonic stem cell-derived $CD34^+$ cells: efficient production in the co-culture with OP9 stromal cells and analysis of lymphohematopoietic potential. *Blood.* 2006;105:617-626.
26. Wang L, Li L, Shojaei F, et al. Endothelial and hematopoietic cell fate of human embryonic stem cells originates from primitive endothelium with hemangioblastic properties. *Immunity.* 2004;21:31-41.

Int. J. Cancer: **120,** 278–284 (2006)

Suppression of ovarian cancer by muscle-mediated expression of soluble VEGFR-1/Flt-1 using adeno-associated virus serotype 1-derived vector

Yuji Takei[1,2], Hiroaki Mizukami[1], Yasushi Saga[2], Ichiro Yoshimura[3], Yoko Hasumi[4], Takeshi Takayama[2], Takahiro Kohno[2], Takashi Matsushita[1], Takashi Okada[1], Akihiro Kume[1], Mitsuaki Suzuki[2] and Keiya Ozawa[1]*

[1]*Division of Genetics Therapeutics, Center for Molecular Medicine, Jichi Medical School, Tochigi, Japan*
[2]*Department of Obstetrics and Gynecology, Jichi Medical School, Tochigi, Japan*
[3]*Department of Urology, National Defense Medical College, Saitama, Japan*
[4]*Department of Obstetrics and Gynecology, University of Tokyo, Tokyo, Japan*

Vascular endothelial growth factor (VEGF) is known to play a major role in angiogenesis in a variety of tumors. A soluble form of Flt-1 (sFlt-1), a VEGF receptor, is potentially useful as an antagonist of VEGF, and accumulating evidences suggest the applicability of sFlt-1 in tumor suppression by means of anti-angiogenesis. We previously demonstrated the efficacy of *sflt-1* gene expression *in situ* to suppress tumor growth and ascites in ovarian cancer. Here, we demonstrate the therapeutic applicability of muscle-mediated expression of sFlt-1 in tumor-bearing mice. Initially, tumor suppressive action was confirmed by inoculating sFlt-1-expressing ovarian cancer (SHIN-3) cells into mice, both subcutaneously and intraperitoneally. To validate the therapeutic efficacy in a more clinically relevant model, adeno-associated virus vectors encoding *sflt-1* were introduced into mouse skeletal muscles and were subsequently inoculated with tumor cells. As a result, high serum sFlt-1 levels were constantly observed, and the growth of both subcutaneously- and intraperitoneally-inoculated tumors was significantly suppressed. No delay in wound healing or adverse events of neuromuscular damage were noted, body weight did not change, and laboratory data, such as those representing liver and renal functions, were not affected. These results indicate that sFlt-1 suppresses growth and peritoneal dissemination of ovarian cancer by the inhibition of angiogenesis, and thus suggest the usefulness of gene therapy for ovarian cancer.

Key words: sFlt-1; AAV; gene therapy; ovarian cancer; VEGF

In recent years, the incidence of ovarian cancer has been on the increase. It is currently the leading cause of death from gynecological cancer.[1] Since the early-stage ovarian cancer is generally asymptomatic, more than half of the patients are diagnosed with the condition at an advanced stage with ascites and peritoneal dissemination.[2] The standard treatment for advanced ovarian cancer is radical cytoreductive surgery followed by combination chemotherapy. Fortunately, ovarian cancer is relatively sensitive to chemotherapy, and a remission can be achieved in a majority of patients, even at the advanced stages.[3,4] Nonetheless, more than half of the patients develop recurrence, and this eventually leads to death, thereby indicating the limitations of the current therapy. Therefore, new strategies are required to improve the therapeutic outcomes.

Angiogenesis is closely related to the development of malignant tumors,[5] and it plays an important role in the growth of primary, metastatic and disseminated lesions of ovarian cancer.[6] Therefore, the inhibition of angiogenesis may suppress peritoneal dissemination, the main mode of progression of ovarian cancer, and may improve the prognosis of advanced ovarian cancer.

The significance of angiogenic factors upon clinical outcome of ovarian cancer have been intensively studied, including vascular endothelial growth factor (VEGF),[7] basic fibroblast growth factor,[8] platelet-derived endothelial cell growth factor (PD-ECGF)[9] and hepatocyte growth factor.[10] Among all, VEGF appears to be the most important and versatile, and it is also reported to be an independent prognostic factor in ovarian cancer patients.[7]

The VEGF-inhibiting factor used in this study was sFlt-1. This is a soluble form of VEGFR-1, and acts as a VEGF antagonist.[11] sFlt-1 is a secretory protein, and systemic expression through circulation can be expected. Main VEGF receptors are Flt-1 and KDR, and both are tyrosine kinase receptors. KDR shows stronger tyrosine kinase activity when the ligand, VEGF, binds, but Flt-1 has stronger VEGF-binding activity.[12,13] Accordingly, when sFlt-1 is present in circulation at a sufficient level, sFlt-1 may competitively inhibit binding of blood VEGF to Flt-1 and KDR, resulting in inhibition of VEGF action.

We have previously demonstrated the tumor suppressive activities of sFlt-1 when it was introduced into ovarian cancer cells.[14] In this study, we aimed at developing a more clinically relevant strategy through a continuous supply of sFlt-1 by muscle-mediated gene transfer using adeno-associated virus (AAV) vectors. AAV vector is derived from a nonpathogenic virus, and a long-term transgene expression can be obtained after intramuscular vector injection.[15–17] Taking these facts into consideration, we began to test the efficacy of the therapeutic approach for ovarian cancer using muscle-mediated *sflt-1* gene expression and compared with the previous strategy which utilized tumor cell transduction.

Material and methods

Cells and plasmids

The human ovarian serous adenocarcinoma cell line SHIN-3[18] was provided by Dr. Y. Kiyozuka (Hyogo College of Medicine, Japan) and used in this study, instead of the previously utilized RMG-1 cells,[14] as the latter cell line did not efficiently form tumors upon inoculation. The SHIN-3 and the human embryonic kidney 293 cell lines were maintained as described previously.[18,19] The murine *sflt-1* cDNA was isolated from the SmaI sites of plasmid psFlt-1,[14] and inserted into the SmaI site of the pCMV-IRES-bsr vector[20] to generate pCMV-sFlt-1-IRES-bsr. Luciferase (LUC)-encoding pCMV-LUC-IRES-bsr[20] was used as a control vector. p2ITR-hsFlt-1 is an sFlt-1 expression plasmid prepared by incorporating human *sflt-1* cDNA into the EcoRI site of pAAV-MCS (Stratagene, La Jolla, CA). Suppression of VEGF-driven HUVEC proliferation by conditioned medium of sFlt-1-expressing cells was already confirmed for both murine[14] and human[21] constructs.

Development of stably transduced cells

Either pCMV-sFlt-1-IRES-bsr or pCMV-LUC-IRES-bsr was introduced into the SHIN-3 cells using the standard calcium phosphate precipitation method.[22] After transfection, the cells were cultured and selected in the presence of 10 μg/ml of blasticidin S hydrochloride (Kaken Pharmaceutical, Tokyo, Japan). After 4 weeks, the blasticidin-resistant SHIN-3/sFlt-1 and SHIN-3/LUC

Grant sponsors: Ministry of Health, Labor and Welfare, Japan; Ministry of Education, Culture, Sports, Science and Technology, Japan; Japan Medical Association. The research award to JMS graduate student.
***Correspondence to:** Division of Genetics Therapeutics, Center for Molecular Medicine, Jichi Medical School, 3311-1 Yakushiji, Minamikawachi, Kawachi, Tochigi 329-0498, Japan. E-mail: kozawa@jichi.ac.jp
Received 18 November 2005; Accepted after revision 7 August 2006
DOI 10.1002/ijc.22307
Published online 25 October 2006 in Wiley InterScience (www.interscience.wiley.com).

Publication of the International Union Against Cancer
uicc global cancer control

cell lines were established and maintained thereafter in the presence of 10 μg/ml of blasticidin S hydrochloride.

AAV vector production

AAV vectors were produced based on the triple plasmid transfection to 293 cells using p2ITR-hsFlt-1, the helper plasmid for adenovirus genes,[23] and the helper plasmid for AAV1.[24,25] A plasmid encoding *lacZ* gene was used to prepare the control AAV vector. The vector stocks were purified using iodixanol (Invitrogen, Carlsbad, CA) density-gradient ultracentrifugation,[24,26,27] and the titer was determined by quantitative DNA dot-blot hybridization.

VEGF quantitation

SHIN-3 cells were inoculated into 10-cm dishes and cultured in a 10% FBS-supplemented DMEM medium. When the cells grew to approximately 80% confluence, the culture supernatant was replaced with serum-free culture medium. After 24 hr, the culture supernatant was recovered. The concentration of VEGF in the supernatant was determined by ELISA System (Amersham Biosciences, Piscataway, NJ).

Western blot analysis

sFlt-1 in the culture supernatant of SHIN-3/sFlt-1 was detected by Western blotting, using standard techniques as described previously.[14] Briefly, the culture supernatant was electrophoresed, transferred into nitrocellulose membrane and incubated with a 1:200 dilution of anti-sFlt-1 polyclonal antibody (provided by Dr. Shibuya). Subsequently, the membrane was reacted with a horseradish peroxidase-labeled secondary antibody, *i.e.*, anti-rabbit antibody (Amersham Biosciences). The bound antibody was visualized by chemiluminescence using an ECL kit (Amersham Biosciences).

In vitro *cell growth kinetics*

SHIN-3/sFlt-1 and SHIN-3/LUC were plated in 6-well plates at a density of 5×10^4 cells/well, and cultured in a 10% serum-supplemented DMEM/F-12 medium. For each group, the cells from a single well were dislodged using 0.05% trypsin-EDTA every 24 hr and were counted using a hemocytometer. This experiment was performed in triplicate.

Tumor cell transduction model

Subcutaneously inoculated tumor growth. Four- to five-week-old female BALB/c nude mice (Japan Clea Laboratories, Tokyo, Japan) were used in the experiment. SHIN-3/sFlt-1 or SHIN-3/LUC cells (5×10^6) were subcutaneously transplanted into the back of the mice, and tumor sizes were measured twice a week using a micrometer caliper. The tumor volume was calculated using the formula: volume = (short diameter)^2 × (long diameter) × 0.5.[28]

Angiogenesis in subcutaneous tumor. On the 21st day after the subcutaneous transplantation of 5×10^6 SHIN-3/sFlt-1 or SHIN-3/LUC cells into the back, the mice were killed and the subcutaneous tumors were excised. After fixation of the tumors in 4% paraformaldehyde, frozen sections were cut, and the endogenous peroxidases were blocked with 3% hydrogen peroxide. The sections were incubated overnight at 4°C with a 1:50 dilution of anti-CD31 antibody (Pharmingen, San Diego, CA) as the primary antibody that recognizes vascular endothelial cells. The sections were then reacted with the secondary antibody, *i.e.*, peroxidase-conjugated anti-rat antibody (Simple Stain Mouse MAX-PO, Rat; Nichirei, Tokyo, Japan) at room temperature for 30 min, followed by color development with diaminobenzidine (DAB). In addition to CD31, immunostaining of von Willbrand factor (vWF) and endothelial nitric oxide synthase (eNOS) was performed. For the specific antibodies, anti-vWF (H-300) and anti-NOS3 (C-20) (Santa Cruz Biotechnology, Santa Cruz, CA) were diluted 50 times, and reacted with the sections at room temperature for 2 hr, followed by color development by DAB reaction using a DAKO LSAB Kit (DAKO, Carpinteria, CA). The number of newly formed vessels was counted under a light microscope at 100× magnification.

Ascites and peritoneal tumor dissemination. SHIN-3/sFlt-1 or SHIN-3/LUC cells (5×10^6) were inoculated into mice intraperitoneally. After 23 days, the mice were killed using diethyl ether, the volume of the ascitic fluid was measured and the peritoneally disseminated lesions were weighed. The volume of ascitic fluid was calculated by subtracting 1 ml from the total volume of fluid that was recovered after the intraperitoneal injection of 1 ml of PBS. The weights of the peritoneally disseminated lesions were calculated by subtracting the weight of the intestine of age-matched, untreated mice from the total weight of the intestine and disseminated lesions removed in one block.

Survival time. SHIN-3/sFlt-1 or SHIN-3/LUC cells (5×10^6) were inoculated into mice intraperitoneally, and the mice were monitored twice daily until they died of massive ascites. Survival rates were calculated using the Kaplan–Meier method.

Therapeutic model using AAV vector

Measurement of serum VEGF and ascitic VEGF. Nude mice were subcutaneously ($n = 5$) or intraperitoneally ($n = 5$) inoculated with SHIN-3 cells (5×10^6 cells), and blood was collected from the tail vein 1, 2, and 3 weeks after inoculation. The serum VEGF level was measured using human VEGF ELISA (R&D system, Minneapolis, MN). Mice that received intraperitoneal SHIN-3 cell inoculation were killed using diethyl ether 3 weeks after inoculation ($n = 3$), ascites were collected, and the ascitic VEGF level was measured by ELISA (R&D system).

Measurement of serum sFlt-1. AAV1-sFlt-1 or AAV1-LacZ vector (2.5×10^{12} genome copy) was given in 10 separate injections into the hind limb skeletal muscles of mice, and the blood samples were obtained from the tail vein every 2 weeks. The concentration of sFlt-1 in the serum was measured using a human sVEGF-R1 ELISA (Bender MedSystems, Vienna, Austria).

Subcutaneously inoculated tumor growth. AAV1-sFlt-1 or AAV1-LacZ vector (2.5×10^{12} genome copy) was injected into the hind limb skeletal muscles of mice. After 9 days, the mice were subcutaneously inoculated with 5×10^6 SHIN-3 cells and monitored thereafter.

Peritoneal tumor dissemination. AAV1-sFlt-1 or AAV1-LacZ vector (2.5×10^{12} genome copy) was injected into the hind limb skeletal muscles of mice. After 9 days, the mice were intraperitoneally inoculated with 5×10^6 SHIN-3 cells. After 23 days later, the mice were killed, and the weights of the intraperitoneally disseminated lesions were measured.

Adverse events. AAV1-sFlt-1 or AAV1 LacZ vectors (2.5×10^{12} genome copies) were injected into the hind limb skeletal muscle of mice. The following experiments were performed to investigate wound healing, neuromuscular damage and body weight changes: Regarding wound healing, a 6-mm square incision was made with scissors in the dorsal skin in nude mice 2 weeks after AAV vector injection, and the healing process was observed with time. As for neuromuscular damage, skeletal muscle of the hind limb at the AAV vector-inoculated site was excised 5 weeks after AAV vector injection, fixed with formalin, paraffin-embedded and sectioned, and the morphology was observed by HE staining. As for body weight changes, body weight of the nude mice was measured before AAV vector injection and 2 and 4 weeks after the administration. Blood was collected 5 weeks after AAV vector injection, and complete blood counts, Alb, BUN, Cr, AST, ALT, Na, K and Cl were measured.

Statistical analysis. Intergroup differences were tested for significance using Student's *t*-test. Survival rates were analyzed by the generalized Wilcoxon and log-rank tests. p values less than 0.05 were considered to be significant.

Results

Detection of VEGF and sFlt-1 in culture supernatants

The concentration of VEGF in the culture supernatant of SHIN-3 cells was 600 pg/ml. sFlt-1 was detected by Western blotting only in the culture supernatant of SHIN-3/sFlt-1 (data not shown).

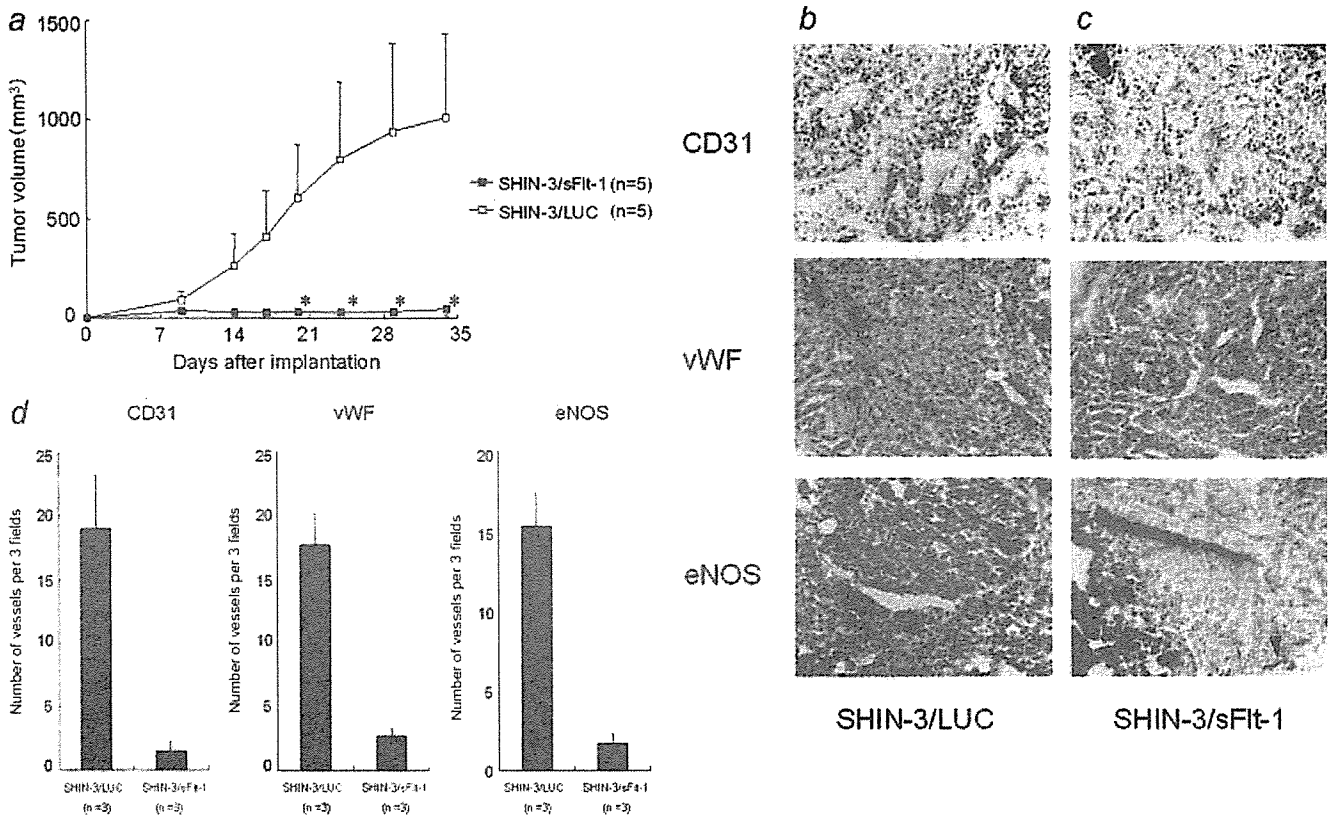

FIGURE 1 – (*a*) *In vivo* tumor growth of sFlt-1-expressing SHIN-3 cells. Tumor cells were subcutaneously injected into the back of mice, and the tumor size was measured every 3 days. The tumor size of SHIN-3/sFlt-1 (■) was significantly smaller than that of SHIN-3/LUC (□, $p < 0.01$ (*)). The tumor volume was calculated using the formula: $(\text{width})^2 \times (\text{length}) \times 0.5$ (mm^3). The data represent the mean ± SD. (*b* and *c*) Immunostaining of subcutaneous tumors of SHIN-3/LUC (*b*) and SHIN-3/sFlt-1 (*c*) with anti-CD31 antibody (upper), anti-vWF antibody (middle) and anti-eNOS antibody (bottom). Endothelial cells of newly formed vessels (arrowhead) were stained dark brown. (*d*) The numbers of new blood vessels in SHIN-3/sFlt-1 and SHIN-3/LUC subcutaneous tumors on the 21st day after inoculation. The number of new blood vessels in SHIN-3/sFlt-1 tumors was significantly smaller than that in SHIN-3/LUC tumors (anti-CD31 antibody; 1.5 ± 0.7 *versus* 19 ± 4, $p < 0.05$, anti-vWF antibody; 2.7 ± 0.6 *versus* 17.7 ± 2.5, $p < 0.01$, anti-eNOS antibody; 1.7 ± 0.6 *versus* 15.3 ± 2.1, $p < 0.01$). Each bar represents the mean ± SD.

In vitro *cell growth kinetics*

The effects of sFlt-1 gene expression on *in vitro* cell growth were examined. There were no differences in growth between SHIN-3/sFlt-1 and the control (SHIN-3/LUC), indicating that the expression of the *sflt-1* gene does not affect *in vitro* cell growth kinetics (data not shown).

Tumor cell transduction model

Subcutaneously inoculated tumor growth. As shown in Figure 1*a*, subcutaneous tumor growth was markedly suppressed in cells expressing sFlt-1. The size of subcutaneous tumors on the 34th day after the transplantation of SHIN-3/sFlt-1 cells was significantly smaller than that of control (43 ± 37 mm^3 *versus* 1004 ± 421 mm^3, $p < 0.01$).

Angiogenesis in subcutaneous tumor. Typical immunohistochemistry of tumors determined using anti-CD31 antibody, anti-vWF antibody and anti-eNOS antibody is shown in Figures 1*b* and 1*c*, and the number of new vessels is summarized in Figure 1*d*. The number of new vessels was significantly smaller in SHIN-3/sFlt-1 than that in control (anti-CD31 antibody; 1.5 ± 0.7 *versus* 19 ± 4, $p < 0.05$, anti-vWF antibody; 2.7 ± 0.6 *versus* 17.7 ± 2.5, $p < 0.01$, anti-eNOS antibody; 1.7 ± 0.6 *versus* 15.3 ± 2.1, $p < 0.01$).

Ascites and peritoneal tumor dissemination. The effects of *sflt-1* gene expression on peritoneal dissemination *in vivo* are shown in Figure 2*a*. The mean volume of ascitic fluid on the 23rd day after intraperitoneal inoculation of SHIN-3/sFlt-1 cells was significantly smaller than that of control (Fig. 2*b*; 0.17 ± 0.13 ml *versus* 1.67 ± 0.71 ml, $p < 0.01$). Similarly, the number of metastasis (Fig. 2*c*) and mean weight of the peritoneally disseminated SHIN-3/sFlt-1 tumors was significantly lower than that of control (Fig. 2*d*; 0.48 ± 0.29 g *versus* 2.74 ± 0.54 g, $p < 0.001$). Thus, *sflt-1* gene expression suppressed ascites production and peritoneal dissemination.

Survival time. The survival of mice was monitored after inoculating tumor cells intraperitoneally. In the control group, the accumulation of ascitic fluid became prominent from the 14th day after inoculation, and all mice died by the 46th day. In contrast, in the SHIN-3/sFlt-1 group, ascitic fluid accumulation was suppressed, resulting in a significantly longer survival (Fig. 2*e*, $p < 0.05$). Therefore, *sflt-1* gene expression prolonged the survival of mice with peritoneal dissemination of ovarian cancer.

Therapeutic model using AAV vector

Serum VEGF concentration and ascitic VEGF concentration. The serum VEGF level was lower than the detection limit in both the subcutaneous and intraperitoneal inoculation groups. In contrast, the ascitic VEGF level was very high (30 ± 9 ng/ml).

Serum sFlt-1 concentration. Following the injection of AAV1-sFlt-1 vector into the mouse skeletal muscles, serum sFlt-1 levels were higher than 1,000 pg/ml throughout the observation period, whereas in the control group with AAV1-LacZ vector, the levels were below the detection limit (Fig. 3*a*).

Tumor growth. The efficacy of muscle-mediated sFlt-1 expression was evaluated in both subcutaneously- and intraperitoneally-transplanted SHIN-3 tumor cell growth. As shown in Figure 3*b*, a

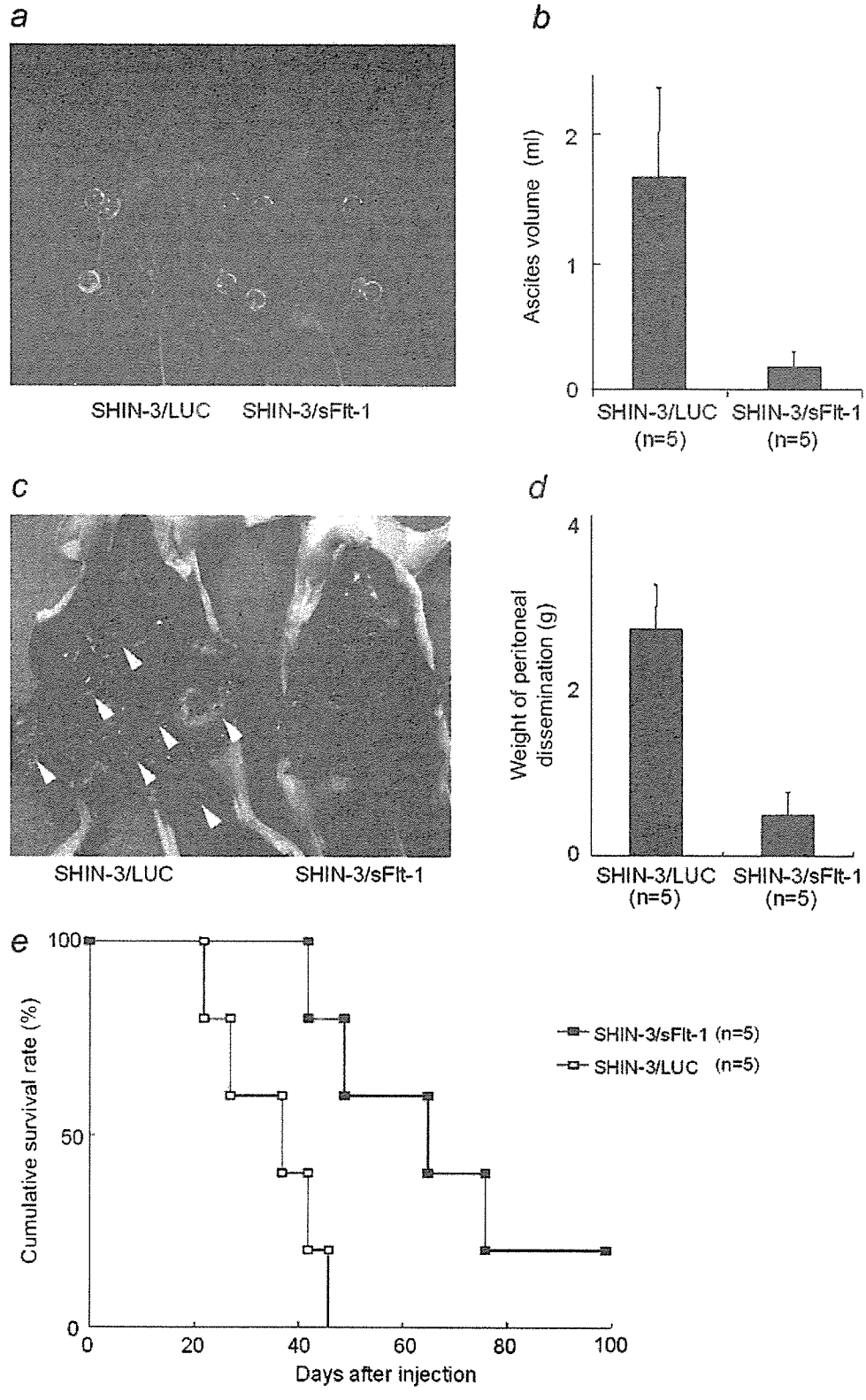

FIGURE 2 – (*a* and *b*) Ascites fluid accumulation on the 23rd day after the intraperitoneal inoculation of cancer cells. Large amounts of bloody ascitic fluid were observed in the SHIN-3/LUC group, whereas in the SHIN-3/sFlt-1 group, the accumulation of ascitic fluid was significantly suppressed (1.67 ± 0.71 ml *versus* 0.17 ± 0.13 ml, $p < 0.01$). (*c* and *d*) Peritoneal dissemination on the 23rd day after peritoneal inoculation of cancer cells. In the SHIN-3/LUC group, marked peritoneal dissemination was observed, particularly on the intestinal surface (arrowheads), whereas in the SHIN-3/sFlt-1 group, peritoneal dissemination was significantly suppressed (2.74 ± 0.54 g *versus* 0.48 ± 0.29 g, $p < 0.001$). (*e*) Kaplan–Meier analysis after intraperitoneal inoculation of cancer cells. Survival was significantly prolonged in the SHIN-3/sFlt-1 group, when compared with that in the SHIN-3/LUC group ($p < 0.05$).

significant suppression of tumor growth was observed in the sFlt-1 injected group ($p < 0.05$). In mice with peritoneal dissemination, the total weight of the peritoneally disseminated lesions on the 23rd day after inoculation was significantly lower than that of control group (Fig. 3*c*; 1.07 ± 0.87 g *versus* 3.15 ± 2.10 g, $p < 0.05$). Therefore, a therapeutic effect was observed in both models.

Survival time. The survival of mice was monitored in both groups. The animals showed accumulation of ascites, and the mean survival lengths were 28.2 and 30.1 days for AAV-LacZ- and AAV-sFlt-1-injected group, respectively. Although the survival in AAV-sFlt-1 group was longer than the controls, statistic significance was not recognized between these groups.

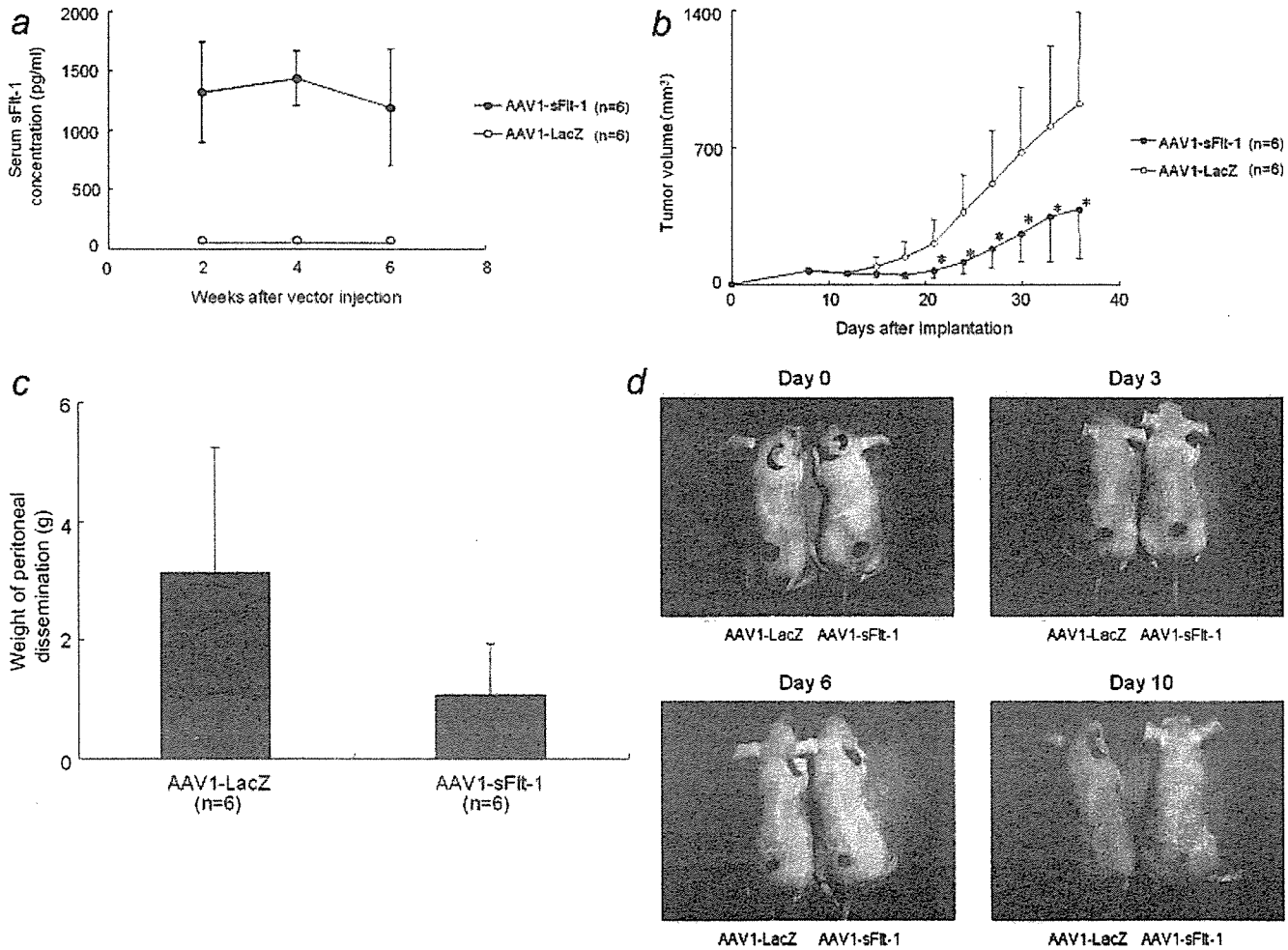

FIGURE 3 – (*a*) Serum sFlt-1 concentrations. In the mice that were intramuscularly injected with AAV1-sFlt-1, the serum sFlt-1 concentration was higher than 1,000 pg/ml. In contrast, in the mice that were intramuscularly injected with AAV1-LacZ, the serum sFlt-1 concentration was below the detection limit. (*b*) Growth of SHIN-3 subcutaneous tumors in the mice that were intramuscularly injected with AAV1-sFlt-1 or AAV1-LacZ. The growth of subcutaneous tumors was significantly suppressed in the intramuscular AAV1-sFlt-1 injection group, compared with that in the intramuscular AAV1-LacZ injection group. The sizes of subcutaneous tumors on the 36th day after the transplantation of SHIN-3 cells in the AAV1-sFlt-1 and AAV1-LacZ groups were 380 ± 250 mm^3 and 921 ± 466 mm^3, respectively (*, $p < 0.05$). (*c*) The total weight of peritoneally disseminated tumors on the 23rd day after the intraperitoneal inoculation of SHIN-3 cells in the mice that had been intramuscularly injected with AAV1-sFlt-1 or AAV1-LacZ. The peritoneal dissemination was significantly suppressed in the AAV1-sFlt-1 group, when compared with that in the AAV1-LacZ group (1.07 ± 0.87 g *versus* 3.15 ± 2.10 g, $p < 0.05$). (*d*) A 6-mm square injury was made in the dorsal region 2 weeks after intramuscular injection of AAV1-sFlt-1 or AAV1-lacZ into nude mice. Photographs of typical views immediately and 3, 6 and 10 days after skin incision are presented. No significant difference was noted between the groups.

Adverse events. Regarding wound healing, the wound was completely repaired about 2 weeks after skin incision in both the AAV1-sFlt-1 ($n = 3$) and control ($n = 3$) groups, showing no significant difference in the time required for healing between the groups. Photographs of typical views immediately and 3, 6, and 10 days after skin incision are shown in Figure 3*d*. As for neuromuscular damage, no apparent damage was noted at the histological level in the AAV1-sFlt-1 group, similar to the control group (data not shown). The body weights were 17.1 ± 1.0, 21.5 ± 0.9, and 23.3 ± 1.2 g before intramuscular AAV vector injection and 2 and 4 weeks after the injection, respectively, in the AAV1-sFlt-1 group ($n = 5$) and 16.9 ± 1.2, 20.7 ± 1.8, and 23.0 ± 1.9 g, respectively, in the control group ($n = 5$), showing no significant difference. The laboratory data are shown in Table I. There were no significant differences in the serum Alb, BUN, Cr, AST, ALT, Na, K or Cl level between the AAV1-sFlt-1 and control groups, nor were there significant differences in the complete blood counts.

Discussion

In this study, we demonstrated the efficacy of muscle-mediated sFlt-1 expression using AAV vectors in both subcutaneous and intraperitoneally disseminated tumors.

A VEGF receptor, Flt-1, consists of an intracellular tyrosine kinase domain, transmembrane domain and extracellular domain, containing 7 immunoglobulin-like domains. sFlt-1 generated by alternative splicing of the Flt-1 gene lacks the intracellular tyrosine kinase and transmembrane domains, and consists of an extracellular domain containing 6 immunoglobulin-like domains, from which the 7th immunoglobulin-like domain is deleted. The VEGF-binding site of Flt-1 is located on the 2nd and 3rd immunoglobulin-like domains in the extracellular domain.[29,30] Hence, sFlt-1 has VEGF-binding ability. However, it has no signal transduction activity because the molecule is not anchored on the cell surface, and lacks the tyrosine kinase do-

TABLE I – LABORATORY DATA

	AAV1-LacZ (n = 3)	AAV1-sFlt-1 (n = 3)	p
WBC (10^3/μl)	1.7 ± 0.3	1.4 ± 0.5	n.s.
Hemoglobin (g/dl)	12.3 ± 1.0	13.9 ± 1.3	n.s.
Platelets (10^4/μl)	75 ± 49	96 ± 42	n.s.
Albumin (g/dl)	0.5 ± 0.1	0.5 ± 0	n.s.
BUN (mg/dl)	36 ± 5	29 ± 4	n.s.
Creatinine (mg/dl)	0.25 ± 0.03	0.19 ± 0.04	n.s.
AST (IU/l)	103 ± 34	86 ± 30	n.s.
ALT (IU/l)	37 ± 5	31 ± 2	n.s.
Na (meq/l)	153 ± 2	154 ± 2	n.s.
K (meq/l)	4.1 ± 0.4	4.2 ± 0.1	n.s.
Cl (meq/l)	116 ± 2	116 ± 2	n.s.

AST, aspartate aminotransferase; ALT, alanine aminotransferase; n.s., not significant.

main. Therefore, sFlt-1 acts as a VEGF antagonist by competing with the original VEGF receptors, Flt-1 and KDR.

Studies suggesting the therapeutic efficacy with sFlt-1-encoding adenoviral vectors for lung[31] or pancreatic[32] cancer have been reported. Our strategy is aimed at attaining long-term sFlt-1 expression not only for tumor suppression but also to prevent the potential recurrence of the tumor after surgical excision. For this purpose, AAV vector appears to be ideal, since transgene expression can be achieved for a number of years.[16,17,24] To date, various serotypes of AAV (1 through 11) have been identified, and the applicability of these serotype-derived vectors has been investigated.[25,33–39] In case of muscle transduction, AAV1-based vector was shown to be more efficient than the rest of the serotypes.[24,25] Therefore, we used AAV1 vectors for *sflt-1* gene transfer. In fact, we had previously attempted the same set of experiments using vectors AAV2 and AAV5; however, none of these experiments showed any promising results (data not shown).

In this study, we confirmed the tumor-suppressive actions of sFlt-1 by transducing tumor cells as we reported in different cell line[14] and demonstrated the therapeutic efficacy of muscle-directed *sflt-1* gene transfer in the tumor-bearing mouse model. Although the muscle transduction model is clinically more relevant, the tumor suppressive action observed in this model was less complete, as assessed by tumor growth (Figs. 1*a vs.* 3*b*), tumor volume (Figs. 2*d vs.* 3*c*) and overall survival. The difference in therapeutic outcome seems to lie in the concentration of sFlt-1 within tumor and the surrounding area. Therefore, in order to obtain more substantial therapeutic benefit, approaches to enhance the supply of sFlt-1 from the muscle by either increasing the vector dose or by transducing more muscle tissues would be necessary. Another approach, increasing the intraperitoneal concentrations of sFlt-1, would be also helpful to improve the therapeutic outcome. However, peritoneal dissemination was inhibited at a concentration of 1,000 pg/ml in this experiment. AAV vectors have an advantage of long-term gene expression, unlike adenovirus vectors, and the level could be maintained at 1,000 pg/ml or higher for as long as 6 weeks in this experiment. The persistent sFlt-1 gene expression may have contributed to the inhibition of peritoneal dissemination. For clinical application, combination of available anticancer drugs and AAV1-sFlt-1 may be recommended more than administration of AAV1-sFlt-1 alone.

Molecular targeted therapy against VEGF has been conducted by using a variety of different molecules.[40–45] Of all these molecules, bevacizumab, an anti-human VEGF monoclonal antibody, appears to be most promising, and clinical trials are ongoing for patients with cancer.[40,42,45] Significant prolongation of progression-free survival was noted in clinical trials with bevacizumab for metastatic colorectal[42] and renal[45] cancer, either in combination with chemotherapy or independently. On the other hand, this strategy requires frequent infusion of drugs, and the adverse effects due to the use of the monoclonal antibody have been noted.[45] Although difficult to predict, our approach may be safer, since it eliminates inherent problems that arise during the repetitive injection of a monoclonal antibody. However, an influence on vascular endothelial cells in normal tissues is a concern as an adverse drug reaction of angiogenesis inhibitors including sFlt-1. Actually, an anti-human VEGF monoclonal antibody, bevacizumab, has been reported to exhibit adverse events of proteinuria, hypertension, nasal bleeding and hematuria.[45] The mechanism of proteinuria is assumed to be injuries of kidney glomerular endothelial and epithelial cells due to bevacizumab-induced reduction of the blood VEGF level.[46] A delay in wound healing has also been reported.[47] However, no delay in wound healing, neuromuscular damage or body weight changes were noted in our experiment, nor were there changes in the laboratory data, and no apparent AAV1-sFlt-1-induced adverse event was observed.

Reports on gene therapy for ovarian cancer that are underway include the use of adenoviral vectors encoding tumor suppressor genes p53[48] and phosphatase and tensin homolog deleted on chromosome 10.[49] These studies aimed at destroying cancer cells by introducing a therapeutic gene into the cancer cells. However, these methods are unrealistic, since introducing a therapeutic gene into all of the peritoneally disseminated cancer cells is impractical. On the other hand, targeted therapy against VEGF is advantageous because it not only has tumor-suppressive effects but also controls the formation of ascites, since it simultaneously suppresses enhanced vascular permeability.[14,50] Theoretically, molecular targeted therapy against VEGF is effective against high VEGF-producing tumors. It is demonstrated that approximately half of the ovarian cancer patients have elevated serum VEGF level.[7] Therefore, this approach would be suitable for at least half of the patients with ovarian cancer. In case of patients who have ovarian cancer with low VEGF-producing tumors, an alternative strategy should be applied. The results of our *in vitro* study suggests that low VEGF-producing ovarian cancer cell lines frequently secrete other angiogenic factors such as PDGF, PD-ECGF and interleukin-8 (unpublished observations). Therefore, a different therapeutic strategy based on the increased level of another angiogenic factor may prove useful for treating patients with low VEGF-producing tumors.

In summary, the experiments using transduced cancer cells confirmed that sFlt-1 has angiogenesis-suppressing activity, through which it inhibits the growth of subcutaneously transplanted ovarian cancer cells and the peritoneal dissemination of tumors. In addition, the *in vivo* experiment that aimed at the clinical application of gene therapy using the AAV vector (AAV1-sFlt-1) revealed that the intramuscular injection of AAV1-sFlt-1 had similar inhibitory effects. These results suggest the possibility of implementing gene therapy using AAV1-sFlt-1 aimed at suppressing peritoneal dissemination of ovarian cancer.

References

1. Jemal A, Tiwari RC, Murray T, Ghafoor A, Samuels A, Ward E, Feuer EJ, Thun MJ. Cancer statistics, 2004. CA Cancer J Clin 2004;54:8–29.
2. Heintz AP. Surgery in advanced ovarian carcinoma: is there proof to show the benefit? Eur J Surg Oncol 1988;14:91–9.
3. McGuire WP, Hoskins WJ, Brady MF, Kucera PR, Partridge EE, Look KY, Clarke-Pearson DL, Davidson M. Cyclophosphamide and cisplatin compared with paclitaxel and cisplatin in patients with stage III and stage IV ovarian cancer. N Engl J Med 1996;334:1–6.
4. Takei Y, Suzuki M, Ohwada M, Saga Y, Kohno T, Machida S, Sato I. A feasibility study of paclitaxel and carboplatin therapy in Japanese patients with epithelial ovarian cancer. Oncol Rep 2003;10: 951–5.
5. Folkman J. Angiogenesis in cancer, vascular, rheumatoid and other disease. Nat Med 1995;1:27–31.
6. Roszkowski P, Wronkowski Z, Szamborski J, Romejko M. Evaluation of selected prognostic factors in ovarian cancer. Eur J Gynaecol Oncol 1993;14 (Suppl):140–5.
7. Cooper BC, Ritchie JM, Broghammer CL, Coffin J, Sorosky JI, Buller RE, Hendrix MJ, Sood AK. Preoperative serum vascular endothelial growth factor levels: significance in ovarian cancer. Clin Cancer Res 2002;8: 3193–7.

8. Davidson B, Goldberg I, Gotlieb WH, Kopolovic J, Ben-Baruch G, Nesland JM, Reich R. The prognostic value of metalloproteinases and angiogenic factors in ovarian carcinoma. Mol Cell Endocrinol 2002; 187(1/2):39–45.
9. Watanabe Y, Nakai H, Ueda H, Nozaki K, Hoshiai H, Noda K. Platelet-derived endothelial cell growth factor predicts of progression and recurrence in primary epithelial ovarian cancer. Cancer Lett 2003;200: 173–6.
10. Sowter HM, Corps AN, Smith SK. Hepatocyte growth factor (HGF) in ovarian epithelial tumour fluids stimulates the migration of ovarian carcinoma cells. Int J Cancer 1999;83:476–80.
11. Kendall RL, Thomas KA. Inhibition of vascular endothelial cell growth factor activity by an endogenously encoded soluble receptor. Proc Natl Acad Sci USA 1993;90:10705–9.
12. Sawano A, Takahashi T, Yamaguchi S, Aonuma T, Shibuya M. Flt-1 but not KDR/Flk-1 tyrosine kinase is a receptor for placenta growth factor (PlGF), which is related to vascular endothelial growth factor (VEGF). Cell Growth Differ 1996;7:213–21.
13. Seetharam L, Gotoh N, Maru Y, Neufeld G, Yamaguchi S, Shibuya M. A unique signal transduction from FLT tyrosine kinase, a receptor for vascular endothelial growth factor VEGF. Oncogene 1995;10:135–47.
14. Hasumi Y, Mizukami H, Urabe M, Kohno T, Takeuchi K, Kume A, Momoeda M, Yoshikawa H, Tsuruo T, Shibuya M, Taketani Y, Ozawa K. Soluble FLT-1 expression suppresses carcinomatous ascites in nude mice bearing ovarian cancer. Cancer Res 2002;62:2019–23.
15. Fisher KJ, Jooss K, Alston J, Yang Y, Haecker SE, High K, Pathak R, Raper SE, Wilson JM. Recombinant adeno-associated virus for muscle directed gene therapy. Nat Med 1997;3:306–12.
16. Kessler PD, Podsakoff GM, Chen X, McQuiston SA, Colosi PC, Matelis LA, Kurtzman GJ, Byrne BJ. Gene delivery to skeletal muscle results in sustained expression and systemic delivery of a therapeutic protein. Proc Natl Acad Sci USA 1996;93:14082–7.
17. Xiao X, Li J, Samulski RJ. Efficient long-term gene transfer into muscle tissue of immunocompetent mice by adeno-associated virus vector. J Virol 1996;70:8098–108.
18. Imai S, Kiyozuka Y, Maeda H, Noda T, Hosick HL. Establishment and characterization of a human ovarian serous cystadenocarcinoma cell line that produces the tumor markers CA-125 and tissue polypeptide antigen. Oncology 1990;47:177–84.
19. Graham FL, Smiley J, Russell WC, Nairn R. Characteristics of a human cell line transformed by DNA from human adenovirus type 5. J Gen Virol 1977;36:59–74.
20. Urabe M, Hasumi Y, Ogasawara Y, Matsushita T, Kamoshita N, Nomoto A, Colosi P, Kurtzman GJ, Tobita K, Ozawa K. A novel dicistronic AAV vector using a short IRES segment derived from hepatitis C virus genome. Gene 1997;200(1/2):157–62.
21. Yoshimura I, Mizuguchi Y, Miyajima A, Asano T, Tadakuma T, Hayakawa M. Suppression of lung metastasis of renal cell carcinoma by the intramuscular gene transfer of a soluble form of vascular endothelial growth factor receptor I. J Urol 2004;171(6, Part 1):2467–70.
22. Wigler M, Pellicer A, Silverstein S, Axel R. Biochemical transfer of single-copy eucaryotic genes using total cellular DNA as donor. Cell 1978;14:725–31.
23. Matsushita T, Elliger S, Elliger C, Podsakoff G, Villarreal L, Kurtzman GJ, Iwaki Y, Colosi P. Adeno-associated virus vectors can be efficiently produced without helper virus. Gene Ther 1998;5:938–45.
24. Mochizuki S, Mizukami H, Kume A, Muramatsu S, Takeuchi K, Matsushita T, Okada T, Kobayashi E, Hoshika A, Ozawa K. Adeno-associated virus (AAV) vector-mediated liver- and muscle-directed transgene expression using various kinds of promoters and serotypes. Gene Ther Mol Biol 2004;8:9–18.
25. Xiao W, Chirmule N, Berta SC, McCullough B, Gao G, Wilson JM. Gene therapy vectors based on adeno-associated virus type 1. J Virol 1999;73:3994–4003.
26. Hermens WT, ter Brake O, Dijkhuizen PA, Sonnemans MA, Grimm D, Kleinschmidt JA, Verhaagen J. Purification of recombinant adeno-associated virus by iodixanol gradient ultracentrifugation allows rapid and reproducible preparation of vector stocks for gene transfer in the nervous system. Hum Gene Ther 1999;10:1885–91.
27. Zolotukhin S, Byrne BJ, Mason E, Zolotukhin I, Potter M, Chesnut K, Summerford C, Samulski RJ, Muzyczka N. Recombinant adeno-associated virus purification using novel methods improves infectious titer and yield. Gene Ther 1999;6:973–85.
28. Kung AL, Wang S, Klco JM, Kaelin WG, Livingston DM. Suppression of tumor growth through disruption of hypoxia-inducible transcription. Nat Med 2000;6:1335–40.
29. Keyt BA, Nguyen HV, Berleau LT, Duarte CM, Park J, Chen H, Ferrara N. Identification of vascular endothelial growth factor determinants for binding KDR and FLT-1 receptors. Generation of receptor-selective VEGF variants by site-directed mutagenesis. J Biol Chem 1996;271:5638–46.
30. Tanaka K, Yamaguchi S, Sawano A, Shibuya M. Characterization of the extracellular domain in vascular endothelial growth factor receptor-1 (Flt-1 tyrosine kinase). Jpn J Cancer Res 1997;88:867–76.
31. Takayama K, Ueno H, Nakanishi Y, Sakamoto T, Inoue K, Shimizu K, Oohashi H, Hara N. Suppression of tumor angiogenesis and growth by gene transfer of a soluble form of vascular endothelial growth factor receptor into a remote organ. Cancer Res 2000;60:2169–77.
32. Hoshida T, Sunamura M, Duda DG, Egawa S, Miyazaki S, Shineha R, Hamada H, Ohtani H, Satomi S, Matsuno S. Gene therapy for pancreatic cancer using an adenovirus vector encoding soluble flt-1 vascular endothelial growth factor receptor. Pancreas 2002;25:111–21.
33. Chiorini JA, Kim F, Yang L, Kotin RM. Cloning and characterization of adeno-associated virus type 5. J Virol 1999;73:1309–19.
34. Chiorini JA, Yang L, Liu Y, Safer B, Kotin RM. Cloning of adeno-associated virus type 4 (AAV4) and generation of recombinant AAV4 particles. J Virol 1997;71:6823–33.
35. Gao G, Vandenberghe LH, Alvira MR, Lu Y, Calcedo R, Zhou X, Wilson JM. Clades of adeno-associated viruses are widely disseminated in human tissues. J Virol 2004;78:6381–8.
36. Gao GP, Alvira MR, Wang L, Calcedo R, Johnston J, Wilson JM. Novel adeno-associated viruses from rhesus monkeys as vectors for human gene therapy. Proc Natl Acad Sci USA 2002;99:11854–9.
37. Mori S, Wang L, Takeuchi T, Kanda T. Two novel adeno-associated viruses from cynomolgus monkey: pseudotyping characterization of capsid protein. Virology 2004;330:375–83.
38. Muramatsu S, Mizukami H, Young NS, Brown KE. Nucleotide sequencing and generation of an infectious clone of adeno-associated virus 3. Virology 1996;221:208–17.
39. Rutledge EA, Halbert CL, Russell DW. Infectious clones and vectors derived from adeno-associated virus (AAV) serotypes other than AAV type 2. J Virol 1998;72:309–19.
40. Cobleigh MA, Langmuir VK, Sledge GW, Miller KD, Haney L, Novotny WF, Reimann JD, Vassel A. A phase I/II dose-escalation trial of bevacizumab in previously treated metastatic breast cancer. Semin Oncol 2003;30(5, Suppl 16):117–24.
41. Garofalo A, Naumova E, Manenti L, Ghilardi C, Ghisleni G, Caniatti M, Colombo T, Cherrington JM, Scanziani E, Nicoletti MI, Giavazzi R. The combination of the tyrosine kinase receptor inhibitor SU6668 with paclitaxel affects ascites formation and tumor spread in ovarian carcinoma xenografts growing orthotopically. Clin Cancer Res 2003;9:3476–85.
42. Kabbinavar F, Hurwitz HI, Fehrenbacher L, Meropol NJ, Novotny WF, Lieberman G, Griffing S, Bergsland E. Phase II, randomized trial comparing bevacizumab plus fluorouracil (FU)/leucovorin (LV) with FU/LV alone in patients with metastatic colorectal cancer. J Clin Oncol 2003;21:60–5.
43. Prewett M, Huber J, Li Y, Santiago A, O'Connor W, King K, Overholser J, Hooper A, Pytowski B, Witte L, Bohlen P, Hicklin DJ. Antivascular endothelial growth factor receptor (fetal liver kinase 1) monoclonal antibody inhibits tumor angiogenesis and growth of several mouse and human tumors. Cancer Res 1999;59:5209–18.
44. Wood JM, Bold G, Buchdunger E, Cozens R, Ferrari S, Frei J, Hofmann F, Mestan J, Mett H, O'Reilly T, Persohn E, Rosel J, et al. PTK787/ZK 222584, a novel and potent inhibitor of vascular endothelial growth factor receptor tyrosine kinases, impairs vascular endothelial growth factor-induced responses and tumor growth after oral administration. Cancer Res 2000;60:2178–89.
45. Yang JC, Haworth L, Sherry RM, Hwu P, Schwartzentruber DJ, Topalian SL, Steinberg SM, Chen HX, Rosenberg SA. A randomized trial of bevacizumab, an anti-vascular endothelial growth factor antibody, for metastatic renal cancer. N Engl J Med 2003;349:427–34.
46. Sugimoto H, Hamano Y, Charytan D, Cosgrove D, Kieran M, Sudhakar A, Kalluri R. Neutralization of circulating vascular endothelial growth factor (VEGF) by anti-VEGF antibodies and soluble VEGF receptor 1 (sFlt-1) induces proteinuria. J Biol Chem 2003;278:12605–8.
47. Niethammer AG, Xiang R, Becker JC, Wodrich H, Pertl U, Karsten G, Eliceiri BP, Reisfeld RA. A DNA vaccine against VEGF receptor 2 prevents effective angiogenesis and inhibits tumor growth. Nat Med 2002;8:1369–75.
48. Zeimet AG, Marth C. Why did *p53* gene therapy fail in ovarian cancer? Lancet Oncol 2003;4:415–22.
49. Saga Y, Mizukami H, Takei Y, Ozawa K, Suzuki M. Suppression of cell migration in ovarian cancer cells mediated by PTEN overexpression. Int J Oncol 2003;23:1109–13.
50. Dvorak HF, Brown LF, Detmar M, Dvorak AM. Vascular permeability factor/vascular endothelial growth factor, microvascular hyperpermeability, and angiogenesis. Am J Pathol 1995;146:1029–39.

Leukemia & Lymphoma, August 2006; 47(8): 1613–1617

informa
healthcare

ORIGINAL ARTICLE: CLINICAL

Pleocytosis after hemopoietic stem cell transplantation

TAKAHIRO NAGASHIMA, KAZUO MUROI, CHIZURU KAWANO-YAMAMOTO, TAKUJI MIYOSHI, RAINE TATARA, AKIKO MEGURO, SHIN-ICHIRO FUJIWARA, YOKO OBARA, IEKUNI OH, SATORU KIKUCHI, KAZUYA SATO, TOMOHIRO MATSUYAMA, MASAKI TOSHIMA, KEN OHMINE, KATSUTOSHI OZAKI, MASAAKI TAKATOKU, MASAKI MORI, TADASHI NAGAI, & KEIYA OZAWA

Division of Cell Therapy, Jichi Medical School Hospital, Minamikawachi-machi, Kawachi-gun, Tochigi-ken, Japan

(Received 29 June 2005; accepted 17 September 2005)

Abstract

Frequency and clinical significance of cerebrospinal fluid (CSF) pleocytosis in hemopoietic stem cell (HSC) transplantation were surveyed. Cyclosporine (CSA)- or tacrolimus (FK506)-based regimens were used as graft-vs-host disease (GVHD) prophylaxis in allogeneic HSC transplantation. CSF pleocytosis with or without neurologic symptoms was detected in 12 of 25 patients receiving allogeneic HSC transplants but in none of 11 patients receiving autologous HSC transplants. Of the 12 patients with CSF pleocytosis, only one patient developed leukoencephalopathy later. There was a correlation between CSF cell numbers and trough levels of CSA but not with those of FK506. In patients receiving allogeneic HSC transplants, CSF pleocytosis may be relatively common and may reflect neurologic damage associated with calcineurin inhibitors.

Keywords: *Pleocytosis, hemopoietic stem cell transplantation, calcineurin inhibitors*

Introduction

Neurologic complications accompanied by CSF pleocytosis in patients receiving CSA or FK506 after allogeneic HSC transplantation or organ transplantation have been reported [1–4]. Mild symptoms including tremor, neuralgia, headache or peripheral neuropathy are common; however, some patients experience severe symptoms including psychoses, hallucinations, blindness, seizures, cerebellar ataxia, motoric weakness or leukoencephalopathy [5–7]. Generally, symptoms of CSA- and FK506-related neurotoxicity are reversed by substantially reducing the dosage of the drugs or discontinuing them [5]. We analysed the frequency and clinical significance of CSF pleocytosis in patients receiving a HSC transplant.

Materials and methods

Patients with hematologic malignancies who underwent HSC transplant between February 1990 and July 2004 at Jichi Medical School Hospital were retrospectively surveyed. Patients received lumbar puncture to inject methotrexate to prevent central nervous system disease both before and after HSC transplantation. Exclusion criteria in this study were as follows: central nervous system involvement of disease before or after HSC transplantation and death within 6 months after HSC transplantation. Patients received intrathecal methotrexate injection once just before HSC transplantation and up to four times according to the disease status after HSC transplantation. Since lumbar puncture was performed on the basis of the doctors' decisions, the day of it was different in each patient. CSF cell numbers were counted in all patients and CSF cell cytology was examined in the three samples from three patients. CSF pleocytosis was defined when the total cell number was more than 15 cells per 3 μl. CSA and FK506 were given intravenously at first and then they were given orally. Usually, in hospital, serum CSA and FK506 trough levels were monitored daily

Correspondence: Kazuo Muroi, MD, Division of Cell Therapy, Jichi Medical School Hospital, 3311-1 Yakushiji, Minamikawachi-machi, Kawachi-gun, Tochigi-ken 329-0498, Japan. Tel: 81-285-44-2111. Fax: 81-285-44-5087. E-mail: muroi-kz@jichi.ac.jp

ISSN 1042-8194 print/ISSN 1029-2403 online © 2006 Informa UK Ltd.
DOI: 10.1080/10428190600625836

or every other day, while in out-patient clinic, they were monitored weekly or every 2 weeks. CSA and FK506 blood trough levels were assayed at the same time of CSF collection using the enzyme multiplied immunoassay technique. p-values below 0.05 were considered significant on Mann-Whitney's U test and χ^2 test.

Results

Thirty-six patients were evaluated (Table I): there were no differences in age, gender, intrathecal methotrexate injection and cranial irradiation between the allogeneic HSC transplantation group and the autologous HSC transplantation group. However, cases of acute myeloid leukemia were only included in the allogeneic HSC transplantation group and total body irradiation (TBI)-based regimens as conditioning such as 120 mg kg^{-1} of cyclophosphamide plus 12 Gy of TBI or 180 mg kg^{-1} of melphalan plus 12 Gy of TBI were performed in that group. Only chemotherapy-based regimens were used as conditioning in the autologous HSC transplantation group as reported previously [8]. In the allogeneic HSC transplantation group, most patients received allogeneic bone marrow transplants from HLA-matched unrelated donors. Four patients received allogeneic bone marrow transplants from HLA-identical siblings, one received an allogeneic peripheral blood stem cell transplant from a HLA-identical sister and one received an allogeneic peripheral blood stem cell transplant from a HLA-mismatched mother. High-titer anti-cytomegalovirus (CMV) gammaglobulin for CMV infection prevention was given to most patients of both groups. Antithymocyte globulin (ATG) for rejection and GVHD prevention was given only to seven patients receiving allogeneic HSC transplants. GVHD prophylaxis was provided by short-term methotrexate (MTX) plus CSA or short-term MTX plus FK506.

Table I. Characteristics of the patients.

	Auto	Allo	p-value
No. of Patients	11	25	
Age (years#)	23	22	0.3110
Gender			0.8247
Male	5	14	
Female	6	11	
Disease			0.0369
AML	0	8	
ALL	5	11	
CML	0	2	
NHL	6	4	
Conditioning			<0.0001
TBI-based	0	25	
Non-TBI-based	11	0	
GVHD prophylaxis			
MTX+CSA	ND	14	
MTX+FK506	ND	11	
Transplant			<0.0001
PBSC	11	2	
R-BM	0	4	
U-BM	0	19	
IT before transplantation#	2.0	4.0	0.0821
IT after transplantation#	4.0	2.0	0.5365
Time of IT after transplantation (days#)	167	179	0.6896
Cranial irradiation	1	1	0.5546
ATG	0	7	0.0505
CMV Ig	10	21	0.5546
Follow-up (days#)	2266	2059	0.1103
Outcome			0.1768
Alive	9	24	

Auto, autologous hemopoietic stem cell transplantation; Allo, allogeneic hemopoietic stem cell transplantation; PBSC, peripheral blood stem cell transplantation; R-BMT, related bone marrow transplantation; U-BMT, unrelated bone marrow transplantation; IT, intrathecal methotrexate injection; ATG, anti-thymocyte globulin; CMV, high-titer anticytomegalovirus gammaglobulin; ND, not done; #, median.

As shown in Figure 1, CSF cell numbers in the allogeneic HSC transplantation group were significantly higher than those in the autologous HSC transplantation group (20.9 ± 29.5 vs 3.2 ± 2.4, $p = 0.007$). In the autologous HSC transplantation group, there were no patients with CSF pleocytosis. CSF cells from three patients with pleocytosis were morphologically examined by cytospin preparations. As shown in Figure 2, most of the CSF cells showed normal

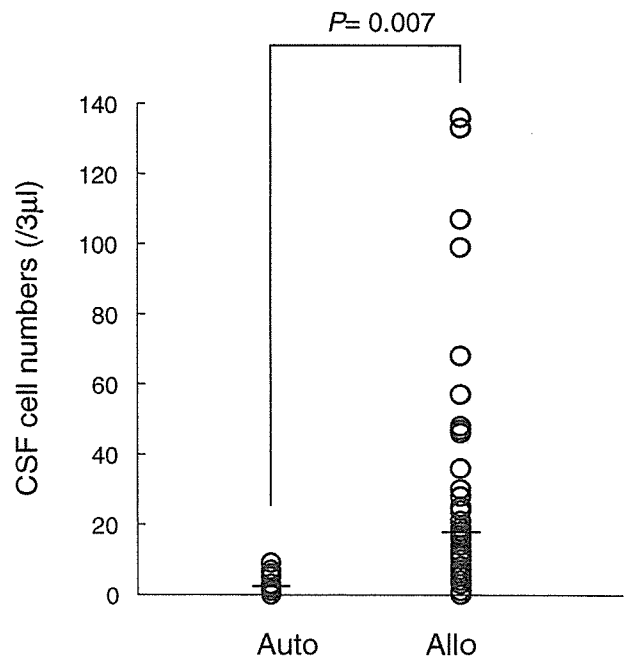

Figure 1. CSF cell numbers in autologous HSC transplantation and allogeneic HSC transplantation. The numbers of analysed CSF samples were 31 in autologous HSC transplantation and 63 in allogeneic HSC transplantation. Auto, autologous HSC transplantation; Allo, allogeneic HSC transplantation.